Remote Sensing of Environment 268 (2022) 112781

Contents lists available at ScienceDirect

Remote Sensing of Environment

journal homepage: www.elsevier.com/locate/rse

Quantifying drought effects in Central European grasslands through regression-based unmixing of intra-annual Sentinel-2 time series

Katja Kowalski [a,*], Akpona Okujeni [a], Maximilian Brell [b], Patrick Hostert [a,c]

[a] Geography Department, Humboldt-Universität zu Berlin, Unter den Linden 6, 10099 Berlin, Germany
[b] Helmholtz Center Potsdam, GFZ German Research Centre for Geosciences, Telegrafenberg, 14473 Potsdam, Germany
[c] Integrative Research Institute of Transformations of Human-Environment Systems (IRI THESys), Humboldt-Universität zu Berlin, Unter den Linden 6, 10099 Berlin, Germany

ARTICLE INFO

Editor: Marie Weiss

Keywords:
Fractional cover
Support vector regression
NDFI
Photosynthetic vegetation
PV
Non-photosynthetic vegetation
NPV
Soil
Copernicus
Climate change

ABSTRACT

Severe droughts caused unprecedented impacts on grasslands in Central Europe in 2018 and 2019. Yet, spatially varying drought impacts on grasslands remain poorly understood as they are driven by complex interactions of environmental conditions and land management. Sentinel-2 time series offer untapped potential for improving grassland monitoring during droughts with the required spatial and temporal detail. In this study, we quantified drought effects in a major Central European grassland region from 2017 to 2020 using a regression-based unmixing framework. The Sentinel-2-based intra-annual time series of photosynthetic vegetation (PV), non-photosynthetic vegetation (NPV), and soil fractional cover provide easily interpretable quantities relevant for understanding drought effects on grasslands. Fractional cover estimates from Sentinel-2 matched in-situ conditions observed during field visits. The comparison to a multitemporal reference dataset showed the best agreement for PV cover (MAE = 7.2%). Agreement was lower for soil and NPV, but we observed positive relationships between fractional cover from Sentinel-2 and the reference data with MAE = 10.1% and MAE = 15.4% for soil and NPV, respectively. Based on the fractional cover estimates, we derived a Normalized Difference Fraction Index (NDFI) time series contrasting NPV and soil cover relative to PV. In line with meteorological and soil moisture drought indices, and with the Normalized Difference Vegetation Index (NDVI), NDFI time series showed the most severe drought impacts in 2018, followed by less severe, but persisting effects in 2019. Drought-specific metrics from NDFI time series revealed a high spatial variability of onset, duration, impact, and end of drought effects on grasslands. Evaluating drought metrics on different soil types, we found that grasslands on less productive, sandy Cambisols were strongly affected by the drought in 2018 and 2019. In comparison, grasslands on Gleysols and Histosols were less severely impacted suggesting a higher drought resistance of these grasslands. Our study emphasizes that the high temporal and spatial detail of Sentinel-2 time series is mandatory for capturing relevant vegetation dynamics in Central European lowland grasslands under drought.

1. Introduction

Grasslands are important agroecosystems of Central Europe. They serve a broad variety of functions and provide a range of ecosystem services, from habitat provision and safeguarding biodiversity to producing forage crops for livestock farming (Bengtsson et al., 2019). However, grasslands are also threatened by impacts of climate change (Chang et al., 2017; Soussana and Lüscher, 2007), and land use intensification or abandonment (Kuemmerle et al., 2016). Meteorological extreme events such as droughts influence grasslands in Europe. With ongoing global climate change, extreme meteorological conditions, such as the consecutive drought in 2018 and 2019, are expected to become more frequent, more severe and longer in the coming years, affecting up to 60% of grasslands across Europe (Hari et al., 2020; Samaniego et al., 2018). Summer droughts specifically decrease grassland yields (Hofer et al., 2016) and influence ecosystem services related to soils and nutrient cycling (Klaus et al., 2020; Walter et al., 2013), to carbon uptake (Ciais et al., 2005), or to faunal and floral species diversity (Barnett and Facey, 2016; Grant et al., 2014).

Remote sensing-based analyses corroborated the high impact of

* Corresponding author.
E-mail address: katja.kowalski@geo.hu-berlin.de (K. Kowalski).

https://doi.org/10.1016/j.rse.2021.112781
Received 15 June 2021; Received in revised form 1 October 2021; Accepted 28 October 2021
Available online 8 November 2021

droughts on different ecosystems across Europe, e.g., during the summer droughts of 2003 and 2018. Vegetation changes such as early senescence and wilting were observed for forests (Schuldt et al., 2020) and croplands (Ciais et al., 2005; Ji and Peters, 2003). Different from other ecosystems, though, immediate and strong drought-induced changes of the vegetation were already apparent shortly after the drought onset in grasslands (Reinermann et al., 2019). Compared to forests, but also croplands, grassland vegetation was found to be more sensitive to changes of climatic water balance during drought years (Buras et al., 2020). Identifying spatial patterns related to complex site-specific factors such as different management intensities (Deléglise et al., 2015; Ingrisch et al., 2018), soil types (Buttler et al., 2019), and species compositions (Hofer et al., 2016) provide a better understanding on grassland vegetation changes during drought periods. Thereby, management strategies of farmers and policy makers can be supported in the light of increasing impacts of droughts in the coming years and decades. Yet, the potential intra-class variability of the drought stress response of grasslands has not yet been quantified from dense and high-resolution Sentinel-2 time series.

A medium spatial resolution of 10-30 m and frequent observations are mandatory to accurately capture the temporal and spatial vegetation dynamics caused by, e.g., management and drought stress (Ali et al., 2016). MODIS and Landsat time series have been used to monitor intra-annual grassland management (Estel et al., 2018; Stumpf et al., 2020) and drought effects on grasslands in Europe (Reinermann et al., 2019; Schuldt et al., 2020). However, the spatial resolution of MODIS (250-500 m) and the observation frequency of Landsat limit spatially detailed intra-annual vegetation assessments. Since 2017, Sentinel-2A/B collect data on medium spatial resolution with an observation frequency of 5 days globally (Drusch et al., 2012), making these data highly suitable for monitoring grasslands (Henebry, 2019). The value of Sentinel-2 for capturing intra-field vegetation dynamics has been demonstrated by mapping biophysical parameters in natural (J. Wang et al., 2019b) and permanent, managed grasslands (Punalekar et al., 2018; Schwieder et al., 2020). Utilizing the temporal frequency of intra-annual Sentinel-2 time series, Griffiths et al. (2020) found that mowing intensity indicated typical, local management patterns across Germany. Similarly, Kolecka et al. (2018) showed that Sentinel-2 time series captured the majority of annual grassland management events. These studies indicate that the improved spatial and temporal resolution of Sentinel-2 opens up new possibilities for accurate and repeated mapping of grassland ecosystems on national to continental scales.

Most commonly, time series of vegetation indices, e.g., the Normalized Difference Vegetation Index (NDVI) or the Enhanced Vegetation Index (EVI), were used to monitor the dynamics of grassland vegetation (a comprehensive overview on remote sensing of grasslands is provided in Reinermann et al., 2020). Time series of vegetation indices are suitable to detect changes of the grassland vegetation caused by management activities, e.g., mowing (Griffiths et al., 2020; Kolecka et al., 2018). However, the interpretation of vegetation index time series is limited to a measure of greenness in a dimensionless unit that can be influenced by, e.g., soil brightness (among others also relating to soil moisture deficits during droughts), colour and texture (Bannari et al., 1995; Gao et al., 2000; Huete et al., 1985; Liu et al., 2012). A vegetation index value as such does not allow differentiation and quantification of physical quantities of, e.g., percent ground cover of different vegetation and non-vegetation land cover fractions (Asner and Heidebrecht, 2002; Xu et al., 2014), or of other biophysical parameters such as Leaf Area Index (LAI) and biomass (Ali et al., 2017; J. Wang et al., 2019b). Creating such physical quantities will instead provide physically-based and thematically interpretable insights into vegetation composition or vegetation productivity over time (Elmore et al., 2000; Numata et al., 2007).

Mapping time series of photosynthetic vegetation (PV), non-photosynthetic vegetation (NPV), and soil fractional cover constitutes a universally applicable framework for characterizing the state and dynamics of land cover in a quantitative way. With regard to grasslands, fractions of PV, NPV, and soil provide comprehensive measures of the essential ground cover components in interpretable quantitative units (Lewińska et al., 2020). The temporal interactions between these components support a better understanding of processes related to management and environmental conditions such as drought (Guerschman et al., 2020). The initial response of grassland vegetation to drought stress is a decrease of leaf water content. A lasting water deficit causes leaf senescence and vegetation dieback (Bayat et al., 2016) resulting in decreasing PV cover and increasing NPV or soil cover. For grasslands, temporally dense information of fractional cover therefore has the potential to improve the understanding of vegetation response to meteorological variability. Vegetation transitions from PV to NPV or soil cover over longer time periods within the growing season are a robust indicator of seasonal drought (Coates et al., 2015; Dennison et al., 2019). To the best of our knowledge, intra-annual fractional cover time series of PV, NPV, and soil derived from Sentinel-2 imagery have not been utilized to analyze drought effects on grasslands in Central Europe.

Multiple approaches exist to estimate ground cover fractions of different surface types from satellite data. With linear spectral mixture analysis (SMA; Adams et al., 1986), cover fractions are estimated as a linear combination of pure endmember spectra weighted by percentage ground cover. Adapting this approach to include endmember variability, Multiple Endmember Spectral Mixture Analysis (MESMA) allows for several models from potential endmember combinations and the best model is determined for each pixel separately (Roberts et al., 1998). SMA and MESMA have been widely applied to map fractional cover of different grassland ecosystems. Using linear unmixing, Asner and Heidebrecht (2002) and Guerschman et al. (2009) assessed the ability of multi- and hyperspectral sensors to estimate PV, NPV, and soil fractions in desert grass- and shrublands, and savanna ecosystems, respectively. Lewińska et al. (2020) used SMA to analyze short- and long-term changes and trends of vegetation cover in the Caucasus with multispectral Landsat data. Similarly, Numata et al. (2007) found that cover fractions derived from a linear mixing model were suitable for monitoring pasture conditions in Brazil. Regression-based unmixing is an alternative approach for fraction mapping. Regression models predict fractions for a cover type based on prior model training with quantitative training samples, i.e., pairs of mixed spectra and related mixing fractions. Few studies using regression-based unmixing so far focused on grasslands. Gessner et al. (2013) predicted fractional cover of different vegetation types and bare surfaces in two Namibian savannas using high resolution training data and random forest regression. Lehnert et al. (2015) found that plant fractional cover on the Tibetan plateau was estimated with the highest agreement to field data by support vector regression models. A general challenge in using regression-based unmixing is the need for quantitative training samples. The use of synthetic training data from spectral libraries (Okujeni et al., 2013) provides a straightforward way to produce such training information. The method of regression-based unmixing with synthetic training data has been applied to map ground cover components of various ecosystems, including shrublands (Suess et al., 2018), forests (Montorio et al., 2020; Senf et al., 2020), urban areas and urban to rural gradients (Okujeni et al., 2018; Schug et al., 2020). Cooper et al. (2020) used the method to quantify fractional cover of multiple vegetated ecosystems including grasslands, however, without a differentiation of grass fractions into PV and NPV cover. Moreover, the approach has been used to derive annual fractional cover time series (Senf et al., 2020; Suess et al., 2018). It has, however, not yet been tested for quantifying intra-annual fractional cover time series of PV, NPV, and soil in European grassland ecosystems.

The overarching goal of our study accordingly was to quantify drought effects in a Central European grassland region during the persisting droughts of 2018 and 2019. We derived fractional cover time series of PV, NPV, and soil from 2017 to 2020 through regression-based unmixing of intra-annual Sentinel-2 time series. We then assessed the capability of Sentinel-2 data to estimate grassland cover fractions by

validating Sentinel-2-based fractional cover results with a reference dataset encompassing grassland cover at multiple phenological stages in the three growing seasons. For a qualitative evaluation, we additionally compared fractional cover estimates to in-situ photographs taken during field visits. Subsequently, we made use of a fraction cover index to emphasize changes in NPV and soil relative to PV as an indicator of drought throughout the time series. We specifically addressed the following research questions:

(1) How reliably can time series of PV, NPV, and soil cover fractions be estimated from Sentinel-2 for grasslands in Central Europe?
(2) How well do time series of a fractional cover-based index reveal drought effects between years?
(3) How did drought effects on grasslands vary spatially during the severe drought from 2018 to 2019?

2. Study area

We developed our method in northeastern Germany, a region rich in grassland and specifically pastureland. Similar to many grasslands in Central Europe, the lowland grasslands in our study area are rainfed and mostly characterized by a moderate productivity (4–6 t/ha; Smit et al., 2008) and management intensity (Estel et al., 2018). The area covers the two federal states of Brandenburg and Mecklenburg Western Pomerania (Fig. 1). Almost half (44.6%) of this area is used for agricultural production with a grassland share of 22.8% (Brandenburg) and 25.2% (Mecklenburg Western Pomerania; Statistisches Bundesamt, 2019). We chose the study area as it represents typical Central European grassland systems. The region is especially vulnerable to climate change impacts, e.g., droughts and decreasing precipitation, as comparably low precipitation levels (<600 mm/year on average; German Weather Service, 2020) meet extensive areas with poor, sandy soils. For the next decades, regional climate simulations indicate shifts in precipitation patterns towards drier summers and increasing temperatures (Enke et al., 2005; Seneviratne et al., 2012). Therefore, growing conditions in northeastern Germany are likely to deteriorate further. Additionally, droughts as observed in, e.g., 2003 and 2018, are expected to occur more frequently as a consequence of climate change (Horton et al., 2015; Seneviratne et al., 2012). In 2018, total annual precipitation was 30–32% lower than the long-term average in our study area (German Weather Service, 2020), which, combined with extraordinarily high temperatures, led to one of the most severe compound drought and heatwave events ever recorded during the summer months. These meteorological conditions heavily affected both natural ecosystems and agricultural lands (Buras et al., 2020). In northeastern Germany, reported grassland yield decreased by 32–48% in 2018 compared to the previous 5 years (Amt für Statistik Berlin-Brandenburg, 2019; Statistisches Amt Mecklenburg-Vorpommern, 2018) indicating massive impacts of droughts on grasslands.

The seasonal development of grassland ecosystems is generally driven by phenological transitions closely linked to temperature and water availability (Bolton et al., 2020; Jin et al., 2019). Variations of water availability and temperature during droughts or heatwaves consequently alter the standard phenological trajectory of grasslands depending on the ecosystem's sensitivity to such changes (de Beurs et al., 2018; Ma et al., 2013). Additionally, management events such as mowing, or grazing represent short-term disturbances of the grassland seasonality. The long-term seasonality of grassland vegetation in our study area is shown based on average MODIS time series for the period from 2000 to 2020 (Fig. 2). The growing season of grasslands usually starts in April (Day-Of-the-Year (DOY) 91) with increasing vegetation growth and photosynthetic activity. During the following months, management events are characterized by vegetation removal (Bahn et al., 2019). After a management event, grassland cover therefore consists of a higher share of exposed soil and remaining dry vegetation. The first period of management activities is visible as declining average NDVI values during the end of May (DOY 150) until the beginning of July (DOY 190). On the plant physiological level, the removal of the aboveground biomass quickly initiates subsequent plant regrowth given

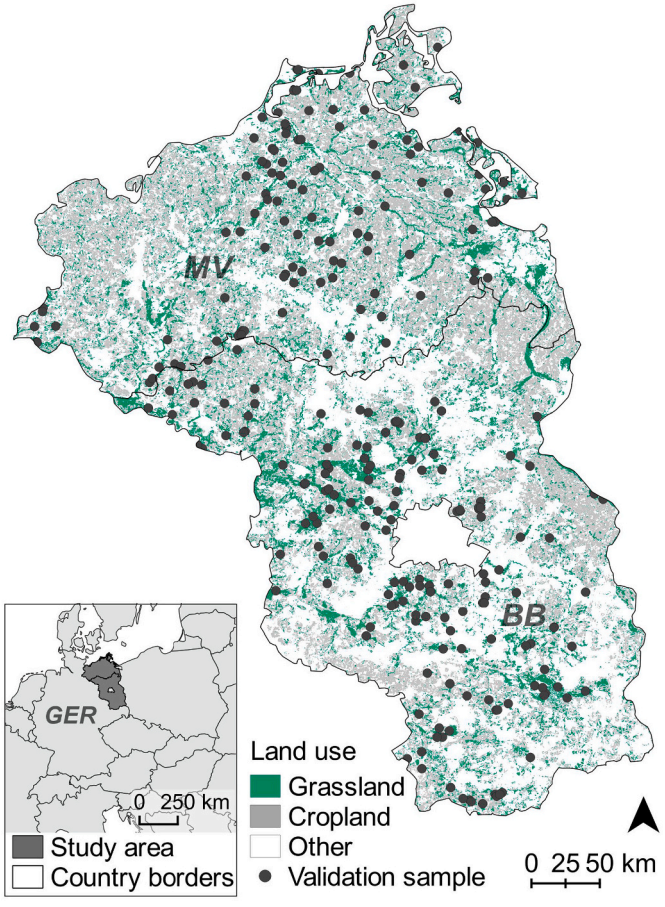

Fig. 1. The study area of northeastern Germany comprising the federal states of Mecklenburg Western Pomerania (MV) and Brandenburg (BB), including validation samples (compare section 3.4). Bottom left: location of the study area within Germany (GER) and Central Europe.

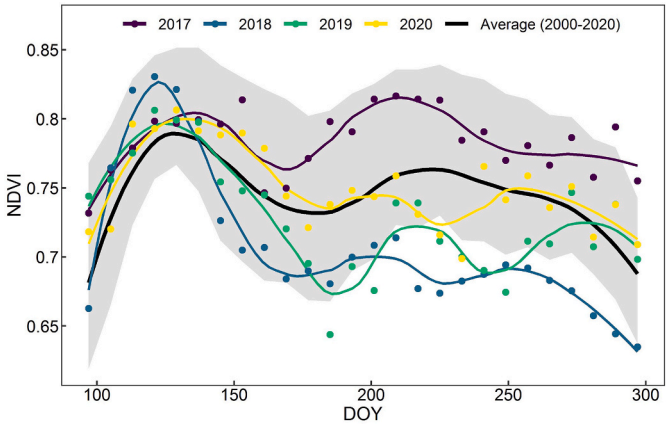

Fig. 2. Average MODIS NDVI time series for grasslands from 2000 to 2020 (grey shading marks the 25th to 75th percentiles) and average time series for the 2017 to 2020 growing seasons. The time series are based on 1000 randomly sampled grassland pixels in the study area. MODIS time series (based on the MOD13Q1 product; Didan, 2015a, 2015b) were downloaded using the Application for Extracting and Exploring Analysis Ready Samples (AppEEARS Team, 2021).

sufficient light, water, and nutrient availability (Gastal and Lemaire, 2015). Consequently, an increase in green vegetation cover is usually following immediately after a management event, which is visible in the average NDVI time series as a second, but weaker green-up between DOY 190 (beginning of July) and DOY 230 (mid-August). While common management periods in grasslands are visible in the average seasonality, individual grassland plots are managed with varying intensity and thus number and timing of management events during the growing season greatly vary in space and time (Griffiths et al., 2020).

Beyond anthropogenic management, extreme meteorological conditions such as drought heavily impact grassland vegetation during the growing season. Effects of long-term drought stress on the plant leaf include decreasing leaf water content, tissue dieback, discoloration and chlorosis of leaves (Bayat et al., 2016). Regarding the vegetation of grasslands, persisting drought stress therefore leads to senescing vegetation and – depending on the vegetation cover density – also to increasing soil cover. These effects are, however, also dependent on abiotic factors and species composition leading to varying responses of grassland vegetation exposed to drought (Beierkuhnlein et al., 2011; Hofer et al., 2016). In the annual NDVI time series (Fig. 2), negative deviations from the average seasonality are particularly apparent from June (DOY 150) until the end of the growing season for 2018 and 2019, indicating prolonged drought effects on the vegetation in these two years. Compared to the long-term average, the growing seasons between April and October had 45.2% and 13.7% lower precipitation in 2018 and 2019, respectively (1991–2020; German Weather Service, 2020). The growing season of 2017 was instead characterized by above average vegetation growth in line with 42.2% above average precipitation. In 2020, the NDVI time series was following the average seasonality during the first half of the growing season. Negative deviations occurred during mid- to late summer (DOY 200–250). During the growing season of 2020, precipitation was 11.1% lower than the long-term average. The four years we investigated in this study represent a wide range of possible vegetation dynamics by covering negative extremes (2018, 2019), positive deviations (2017) and average to dry conditions (2020) compared to the 20-year average seasonality.

3. Data and methods

We used all available Sentinel-2 data for the study period from 2017 to 2020 to derive a four year intra-annual fractional cover time series of PV, NPV, and soil using regression-based unmixing with synthetic training data from spectral libraries (Okujeni et al., 2013, 2017), as detailed in the workflow diagram (Fig. 3). We validated fractional cover from Sentinel-2 at different time steps using a stratified random sampling across the study area. For a qualitative assessment, we compared fractional cover estimates to photographs from in-situ field visits in 2018 and 2019. We then used the fractional cover time series to analyze the grassland response to drought by converting the PV, NPV, and soil estimates into a normalized difference fraction index (NDFI) time series contrasting NPV and soil cover in relation to PV cover. We compared the monthly distributions of NDFI to the NDVI, to two commonly used meteorological drought indices, i.e., the standardized precipitation index (SPI) and the standardized precipitation evapotranspiration index (SPEI), as well as to the soil moisture index (SMI). Subsequently, we developed a set of metrics based on NDFI time series describing the specific drought response of grassland vegetation within each growing season. Most processing steps including the preprocessing of Sentinel-2, the regression-based unmixing of Sentinel-2, and time series analyses were carried out using the Framework for Operational Radiometric Correction for Environmental monitoring (FORCE, v.3.6.4; Frantz, 2019).

3.1. Preprocessing of Sentinel-2 data

We obtained all available Sentinel-2 MSI scenes for our study area between 2017 and 2020 from the Copernicus Open Access Hub. We excluded images earlier than 1st April and later than 15th November for all years to limit the analysis to the grassland growing season. We used the Framework for Operational Radiometric Correction and Environmental monitoring (FORCE; Frantz, 2019) to build a Sentinel-2 time series of analysis-ready surface reflectance data. The geometric uncertainty between individual Sentinel-2 images of up to 11 m (European Space Agency (ESA), 2020) can introduce additional noise to a pixel-based time series. We therefore applied a geometric co-registration step during preprocessing within FORCE. The modified Landsat Sentinel Registration (LSReg) algorithm matches each Sentinel-2 image to monthly average Landsat composites over a 5-year period based on tie points detected on different spatial resolutions (Rufin et al., 2020; Yan et al., 2016). We found that NDVI time series noise was reduced by 12.5% when using LSReg, confirming the usefulness of applying an improved co-registration in northeastern Germany. Subsequent radiometric processing corrected atmospheric, topographic and bidirectional reflectance effects based on radiative transfer theory (Frantz, 2019; Frantz et al., 2016a). The six 20 m-bands of the Sentinel-2 Multispectral Imager (MSI) were resampled to match the four visible and near-infrared bands at 10 m resolution using the ImproPhe algorithm (Frantz et al., 2016b). The preprocessing includes cloud and cloud-shadow masking based on an adapted version of the Fmask algorithm (Frantz et al., 2018; Zhu and Woodcock, 2012, 2014). Observations identified as cloud, cloud-shadow or snow were excluded based on the pixel-based quality information. Thereby, the average cloud-free observation frequency within the growing season was 23, 8, 10, and 10 days for 2017, 2018, 2019, and 2020, respectively (Fig. S5). Data were then gridded into 30 × 30 km tiles using Lambert Azimuthal Equal Area projection (Frantz, 2019). We used a 2018 land use classification to mask all pixels which were not identified as grassland (Blickensdörfer et al., 2021). The preprocessed time series of the ten Sentinel-2 bands was used to model fractional cover time series of PV, NPV, and soil.

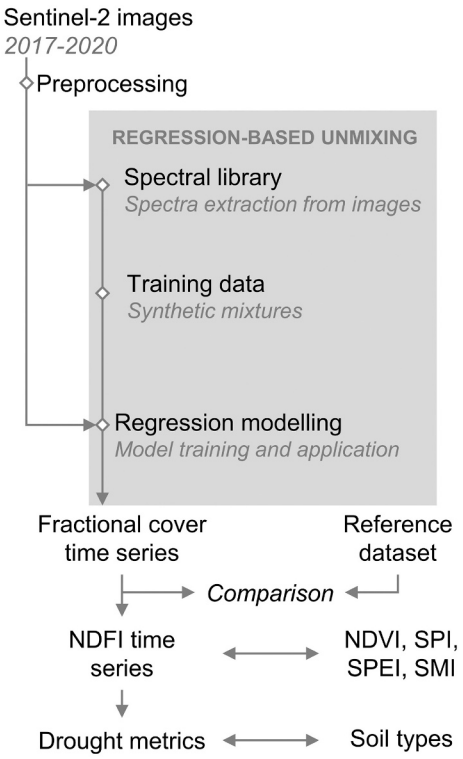

Fig. 3. Workflow diagram for deriving grassland drought metrics.

3.2. Spectral library development

We developed our spectral library based on the NDVI/SWIR ratio feature space concept as proposed by Guerschman et al. (2009). The NDVI separates PV cover with high NDVI values from NPV and soil cover with low NDVI values. The SWIR ratio, calculated as the ratio between SWIR2 and SWIR1, can be used to separate NPV from soil cover and was proposed as multispectral surrogate for the hyperspectral Cellulose Absorption Index (CAI; Daughtry et al., 2005). Consequently, plotting the NDVI versus the SWIR ratio results in a triangular feature space. The pure PV, NPV, and soil surface spectra can be extracted from the vertices of the triangular feature space while mixtures of these cover types are located within the triangle. The shape of the NDVI/SWIR ratio feature space is consistent through space and time. The concept therefore serves as a generalized framework for mapping and monitoring PV, NPV, and soil cover fractions based on single spectral signatures for each cover type (Guerschman et al., 2009).

The triangular NDVI/SWIR ratio feature space throughout our study period is illustrated in Fig. 4. While the overall feature space shape remains consistent through time, changes in the density distribution indicate the seasonal changes of PV, NPV, and soil cover components in our study site. As suggested by Guerschman et al. (2009), we developed our spectral library based on pixel spectra which were located at the vertices of the NDVI/SWIR ratio feature space. To be able to compare changes in PV, NPV, and soil cover fractions consistently through time, we selected a global set of library spectra representative of the entire time series (Fig. 4). For PV, we used one spectral signature from May 2019 as maximum PV cover in grasslands occurs after the start of the season (i.e., in late April to May). For NPV, we selected the spectral signature in July 2019, as NPV cover increases later in the season with senescing grass cover (Gastal and Lemaire, 2015). For soil, we extracted a spectral signature from ploughed cropland next to grassland as open soil cover rarely exists in Central European grasslands. Thereby, the selected spectra represent the maximum cover of each class under Central European climate conditions and land management. We added a virtual shade spectrum with 0% reflectance to the spectral library to account for albedo differences and sub-pixel shading in mixed pixel spectra.

3.3. Regression-based unmixing

We used regression-based unmixing with synthetic training data from spectral libraries (Okujeni et al., 2013, 2017) to estimate fractions of PV, NPV, and soil cover for each image of the Sentinel-2 time series. First, synthetic training data, i.e., pairs of the respective mixed spectrum and its related mixing fraction, were generated for each cover type based on the spectral library. Next, a regression model was trained for each cover type using the synthetic dataset as training data. In a third step, the regression model was applied to the image data to derive a fraction map for each cover type. We iterated the three steps multiple times and

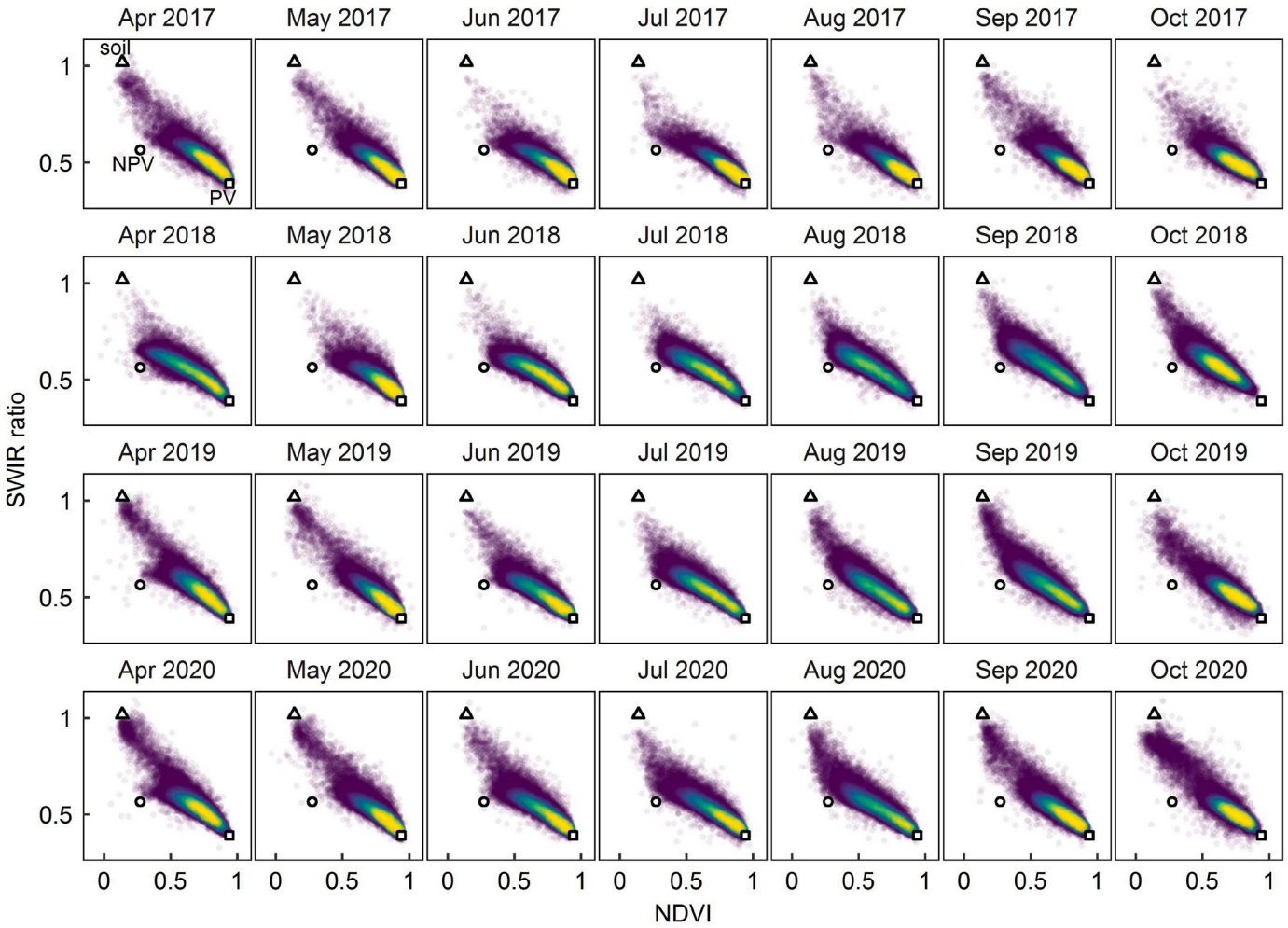

Fig. 4. Location of the global PV, NPV, and soil library spectra in the feature space created by NDVI and SWIR ratio (SWIR2/SWIR1). The distributions of the feature space are based on 30,000 randomly selected pixel observations per month from grasslands in the study area (yellow corresponds to high and purple corresponds to low densities). (For interpretation of the references to colour in this figure legend, the reader is referred to the web version of this article.)

averaged the intermediate maps following Okujeni et al. (2017). Running such an ensemble, a high variability of different mixtures is included while the sample size is kept low.

3.3.1. Generation of synthetic training data

The generation of synthetic training data followed a similar strategy as described in Cooper et al. (2020) and Okujeni et al. (2021). Ten training datasets were generated from the spectral library for each cover type, in the following referred to as 'target class'. Each dataset consisted of 1000 synthetic mixtures. The datasets were generated by mixing library spectra with cover proportions between 0 and 1, i.e., corresponding to 0% and 100%. Covering this full range of proportions in the training set ensures that the regression model is capable of predicting the full potential range of PV, NPV, and soil proportions that may be present in the images to be unmixed, independent from the underlying distribution of proportions. Each of the 1000 synthetic mixtures was created as follows: First, the number of library spectra within the synthetic mixture, i.e., the mixing complexity, was randomly set to two or three. The first library spectrum was the target class spectrum which got assigned a random weight between 0 and 1. The second spectrum (and third spectrum, depending on the mixing complexity) was randomly selected from the remaining classes. Again, cover fractions were assigned randomly as a weight to the remaining mixing components ranging from 0 to 1 under the constraint of creating a sum of 1, i.e., 100%, across all spectra proportions. The final synthetically mixed spectrum was calculated as the linear combination of the weighted library spectra and added together with the mixing fraction of the target class to the training data. The pure library spectra were added to the training data with assigned mixing fractions of 0 or 1.

3.3.2. Support vector regression modeling

We used support vector regression (SVR) to train ten regression models for each class using the synthetic training datasets. SVR is a supervised machine learning algorithm to estimate a continuous target variable based on a set of predictor variables (Awad and Khanna, 2015). The optimal SVR function is fitted by introducing an ε-insensitive area around the regression function where errors smaller than ε are not penalized. Non-linear relationships in the data space are solved by transforming the data into higher-dimensional space using a kernel function. SVR models have a high generalization capability (Smola and Schölkopf, 2004) and performed well for estimating fractional vegetation cover of grasslands (Ge et al., 2018; Lehnert et al., 2015). We used the radial basis function kernel and tuned the model parameters by performing a grid search using 10-fold cross validation as described in van der Linden et al. (2015). We applied the ten respective SVR models to each image of the Sentinel-2 time series to produce ten intermediate fraction maps for each class and observation. Finally, the ten intermediate predictions for each class and observation were averaged to produce the PV, NPV, and soil fractional cover time series from Sentinel-2.

3.4. Validation of fractional cover time series

We used reference fractional cover information derived by visual interpretation of very high-resolution (VHR) images to validate the Sentinel-2-based fractional cover time series. Using VHR imagery for validation of fractional cover from multispectral data has proven a useful method in studies investigating, e.g., multiple vegetation growth forms (Cooper et al., 2020; Lippitt et al., 2018) as well as PV, NPV, and soil fractional cover (Roberts et al., 2012). To generate the reference dataset, we made use of a stratified random sampling design capturing the value range of PV, NPV, and soil fractional cover. We first digitized the spatial extents of all available VHR images available in Google Earth Pro © for our study area from April to mid-November 2017, 2018, 2019, and 2020, respectively. Overall, images were available during 19 different observation dates covering 84% of grasslands in the study area (Fig. 1). Next, we created NDVI and SWIR ratio composites of all available Sentinel-2 images within a maximum of 5 days before and after the VHR acquisition dates (Table S1). We used the nearest observation if more than one observation was available. The stratified sample was built by randomly sampling 25 Sentinel-2 pixels within each 0.2 NDVI and SWIR ratio step (Fig. 5a). PV, NPV, and soil reference fractional cover for each Sentinel-2 pixel was estimated based on a grid sampling approach. First, each pixel sample was divided into 100 cells of 1 × 1 m (Fig. 5b). Second, the dominant cover type, i.e., PV, NPV, or soil, was assigned to each cell through visual interpretation of the underlying VHR image. And finally, the percentages of the cover types were calculated for the pixel sample. The final reference dataset consisted of 271 samples as we excluded, e.g., samples not fully located in grassland fields.

To validate our fractional cover time series, we calculated the Mean Absolute Error (MAE) and Root Mean Square Error (RMSE) for each cover type based on our estimated and reference PV, NPV, and soil fractional cover. The MAE is the average absolute error between predicted and observed values. It gives equal weights to all deviations. The RMSE is the square root of the mean of all squared deviations and consequently gives more weight to samples with high differences. As a measure of agreement, we additionally used the R^2 to describe the percentage of the variance of the reference fractional cover explained by the variance of Sentinel-2 fractional cover. Additionally, we used slope and intercept of a simple linear regression of the reference data and Sentinel-2 fractional cover to evaluate the agreement along the 1:1 line.

3.5. Assessment of drought stress

3.5.1. Normalized Difference Fraction Index time series and metrics

During a persisting drought, the NPV and soil cover is expected to increase, whereas PV cover will decrease. Following Souza et al. (2005), we adapted the Normalized Difference Fraction Index (NDFI) to express fractional cover proportions of NPV and soil, and PV. The NDFI has been used to characterize forest disturbance processes by contrasting PV relative to the combined soil and NPV fractions (Bullock et al., 2020; Souza et al., 2005):

$$NDFI = \frac{(f_{NPV} + f_{soil}) - f_{PV}}{f_{NPV} + f_{PV} + f_{soil}} \quad (1)$$

where f_{NPV}, f_{soil}, and f_{PV} are the cover fraction estimates of NPV, soil and PV, respectively. In Central European grasslands, the amount of litter varies with different management regimes and with growing conditions in previous years (Huber et al., 2017; Török et al., 2012). Thereby, NPV fractional cover estimates may include residual litter originating from previous years. To only capture the seasonal change of NPV, we adapted the NDFI by subtracting the annual NPV base value from each observation:

$$NDFI = \frac{\left(\left(f_{NPV} - f_{i_{NPVbase}}\right) + f_{soil}\right) - f_{PV}}{\left(f_{NPV} - f_{i_{NPVbase}}\right) + f_{PV} + f_{soil}} \quad (2)$$

The NPV base value $f_{iNPVbase}$ was derived for each growing season separately as the minimum NPV cover fraction observed during April to mid-June of the same year *i*. As vegetation senescence only occurs later in the growing season, i.e., during mid- to late summer, we assume that the minimum NPV fraction during that period represents the remaining NPV proportion from the previous year. The original NDFI (eq. 1) has a value range from −1 to 1. By including the NPV base value, the adjusted NDFI (eq. 2) can exceed the value range, e.g., with NPV and soil cover values close to 0%. Accordingly, NDFI values >1 were set to 1. The NDFI (eq. 2) was calculated for each observation in the fractional cover time series.

By assessing the NPV and soil fractions as NDFI time series in an integrated fashion, the different fractions and how those relate to each other becomes easily interpretable: If NDFI >0, the NPV and soil fractions are the predominant cover compared to the PV fractional cover. When a grassland pixel is predominantly covered by dead plant material

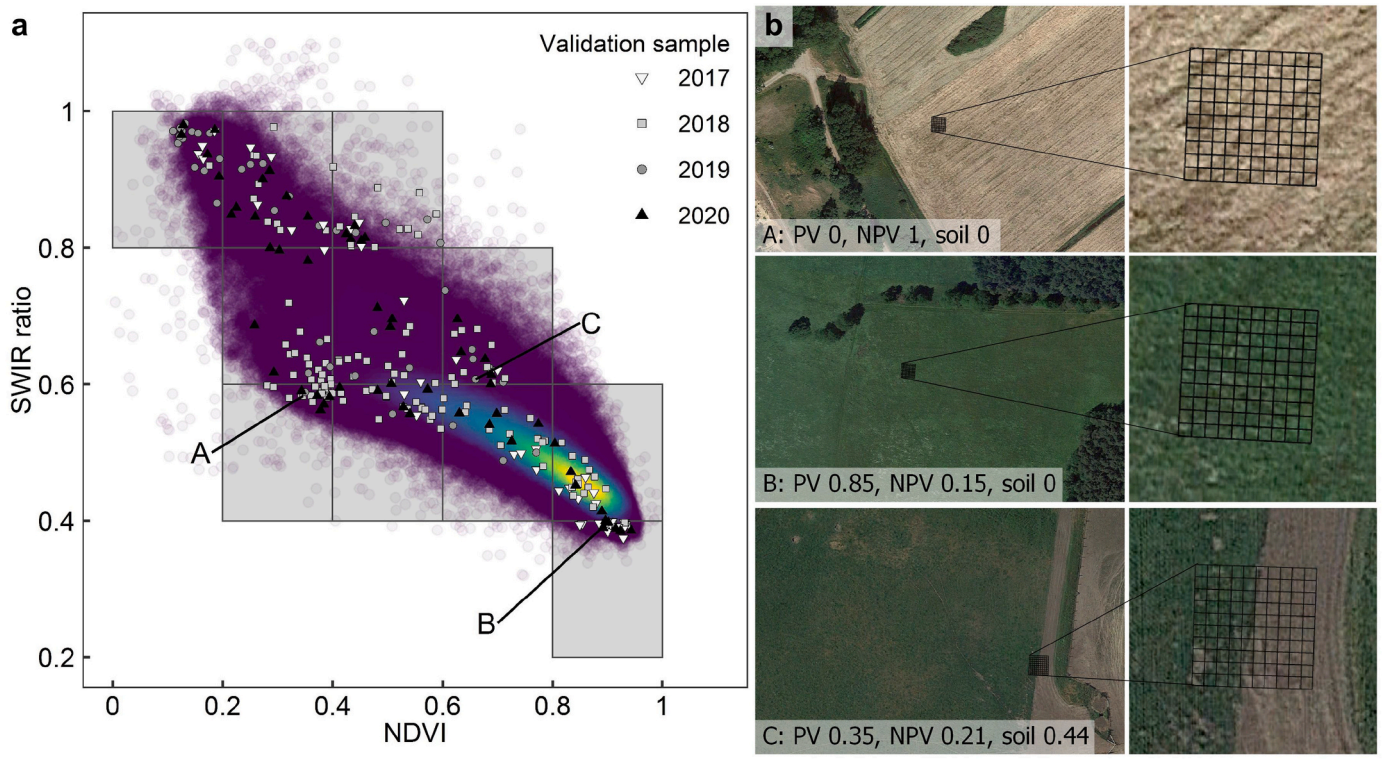

Fig. 5. Feature space of NDVI and SWIR ratio based on Sentinel-2 data close to the acquisition dates of VHR images (a). Twenty-five Sentinel-2 pixels were randomly sampled in each NDVI and SWIR ratio stratum. Three exemplary 10 × 10 m pixel samples and their estimated ground cover based on VHR imagery from Google Earth Pro © (b).

and soil for a time span of at least several weeks or longer within the growing season, this is likely caused by drought stress. Shorter time spans of dominating soil and NPV fractions indicate management disturbances and subsequent regrowth (see section 2 on the relevant processes in Central European grassland regimes).

We captured these differences with temporal metrics characterizing the longest time span of NDFI >0 in each growing season (i.e., duration, day of onset, day of end, mean NDFI). To derive the longest time span of NDFI >0, we used a linearly interpolated time series with daily time steps. Compared to other commonly used interpolation techniques, e.g., radial basis functions (Schwieder et al., 2016) or splines (Bolton et al., 2020), we relied on an approach preserving the minimum and maximum NDFI values in the time series. Preserving the original time series values is beneficial for analyzing time series of Central European grasslands due to their high temporal variability (Griffiths et al., 2020). We first identified potential time periods of NDFI >0 as consecutive observations with a negative and a positive (potential day of start), or a positive and a negative NDFI value (potential day of end). We selected the time span with the longest duration in days and the corresponding day of start and day of end. Then, the mean NDFI during this time span was calculated.

3.5.2. *NDVI time series*

We compared the seasonal dynamics from NDFI time series to the NDVI (Tucker, 1979) as one standard vegetation index used for drought monitoring (West et al., 2019). We derived the NDVI time series from the preprocessed Sentinel-2 data from 2017 to 2020. We calculated monthly NDVI averages for each pixel to enable a comparison to the monthly distributions of the NDFI and to the meteorological drought indices (see section 3.5.3).

3.5.3. *Meteorological drought indices*

We used two common meteorological drought indicators, the Standardized Precipitation Index (SPI; McKee et al., 1993) and the Standardized Precipitation Evapotranspiration Index (SPEI; Vicente-Serrano et al., 2010), as well as the soil moisture index (SMI) to evaluate their distribution in comparison to the NDFI time series. For deriving the SPI and SPEI, we downloaded monthly precipitation and potential evapotranspiration data with 1 km resolution (1970–2020 for SPI and 1990–2020 for SPEI; DWD Climate Data Center (CDC), 2020a, 2020b). We calculated both indices based on a 3-month time window as previous studies have shown that such binning allows assessing seasonal drought effects (Ji and Peters, 2003). For obtaining the SPI, monthly precipitation values were first averaged for each month based on the preceding two months and the actual month. From the aggregated time series, a gamma probability density function was fitted for every month of the year based on the historic record for the respective month. The SPI value was then determined by applying the inverse normal function to the cumulative probability value of each precipitation observation. The SPEI evolved from the SPI by taking a simple climatic water balance, i.e., the difference between precipitation and potential evapotranspiration, into account (Vicente-Serrano et al., 2010). The SPEI is calculated similar to the SPI but instead of the gamma distribution, a log-logistic distribution is used. SPEI and SPI values give an indication of the deviation of the observed value from the long-term median. Values close to 0 consequently indicate average conditions whereas values close to 1 and − 1 indicate wet and dry conditions, respectively. Additionally, we downloaded monthly SMI data (4 km spatial resolution) which is based on the mesoscale Hydrological Model (mHM; Samaniego et al., 2010). The SMI quantifies the percentile of the current soil moisture estimate for the topsoil based on a reconstructed data distribution from 1951 to 2019 (Zink et al., 2016). As the meteorological indices and the SMI are available for each month, we calculated the monthly average NDFI for each pixel. We then compared the monthly distributions of SPI03, SPEI03, and SMI to the monthly NDFI distributions.

3.5.4. *Soil type data*

We further analyzed spatial patterns of the mean NDFI and the duration metric for different soil types. A detailed soil map on the scale

of 1:200,000 was available for the complete study area (Bundesanstalt für Geowissenschaften und Rohstoffe (BGR), 2018). Soil types were derived and aggregated based on soil horizon information according to Eckelmann et al. (2005).

4. Results

4.1. Validation of Sentinel-2 fractional cover estimates

Comparing fractional cover estimated from Sentinel-2 to the reference dataset, we found the overall best agreement for PV, followed by soil and NPV (Fig. 6). For PV, we observed a consistently high agreement close to the 1:1 line with an MAE of 7.2%. Soil estimates from Sentinel-2 show a linear correlation to the reference data with an MAE of 10.1%. Point patterns reveal a slight over- and underestimation in the lowest and highest fraction cover values, respectively. Agreement between NPV fractional cover from Sentinel-2 and the reference dataset was less strong while we still observed a positive correlation. A negative bias of 6.3% indicates that Sentinel-2 generally underestimated NPV fractional cover, while we also observed an overestimation of NPV for low cover values.

4.2. Fractional cover time series from Sentinel-2

The temporal changes of average PV, NPV, and soil fractional cover estimates followed the distinct phenological development of the grassland vegetation in 2017–2020 (Fig. 7). The green-up in spring (April and May) was characterized by strongly increasing PV cover and decreasing NPV and soil fractions across the study area in all years. During the growing season of 2017, PV remained on an overall high level whereas NPV and soil were, on average, below a maximum cover of about 40% and 20%, respectively. In 2018, PV cover decreased strongly during May and June, shortly after the spring green-up. Simultaneously, NPV cover increased and soil cover followed during June. In 2019, PV fractional cover also decreased after peaking in spring, although changes in fractional cover during May and June were not as strong as during the most extreme drought in 2018. Similar dynamics as in 2019 were observed for 2020 with slightly higher PV cover during green-up from May to June. Still, NPV and soil cover increased during the summer months of July and August.

Photographs taken during field visits in 2018 and 2019 confirmed the agreement between estimated fractions from Sentinel-2 and overall vegetation cover conditions (Fig. 8). Our estimates captured changes of the vegetation cover over time related to management and drought. The field in Fig. 8a was grazed during the dry summer months of 2019, resulting in high NPV cover at the end of July (*t1*). After grazing and subsequent mowing, high NPV cover persisted during late August (*t2*) before vegetation regrowth started in mid-September. In Fig. 8b, high PV occurred during vegetation regrowth (*t1*, late July) after a mowing event in late June. In early August, the next mowing event caused a decrease of PV cover along with increasing NPV and slightly increasing soil cover, which was still evident in late August (*t2*). In Fig. 8c, vegetation did not fully recover after the first management event in June 2018. In line with conditions observed on the field, PV fractional cover from Sentinel-2 stayed below ca. 30% during the summer drought with consistently higher NPV and soil fractional cover. In close proximity (< 200 m distance), we observed good growing conditions corroborated by Sentinel-2 fractional cover estimates (Fig. 8d). The corresponding NDFI time series show the relative proportions of NPV and soil to PV cover. Management events in the example sites were characterized well by short increases of NDFI above the threshold of 0 (Fig. 8b, d), whereas NDFI exceeded the threshold for extended time spans on sites with low vegetation growth during drought periods in 2018 and 2019 (Fig. 8a, c). NDVI time series showed very similar seasonal patterns as the NDFI. However, compared to the NDVI, increasing NDFI values are directly linked to increasing NPV and soil fractional cover, e.g., during vegetation changes after management events (Fig. 8b, d) and during drought periods (Fig. 8a, c).

4.3. Seasonal drought impacts on grassland vegetation

The density distributions of monthly NDFI values indicated the highest proportions of NPV and soil relative to PV during the growing season of 2018, followed by 2019, 2020, and 2017 (Fig. 9a). In 2017, mean PV cover remained on a high level during the growing season from May to November indicated by NDFI values below 0 for most of the data distribution. In contrast, most grasslands were covered by a higher proportion of NPV and soil relative to PV from June to the end of 2018, suggesting strong drought effects on the vegetation during the majority of the growing season. In 2019, NPV and soil cover fractions were

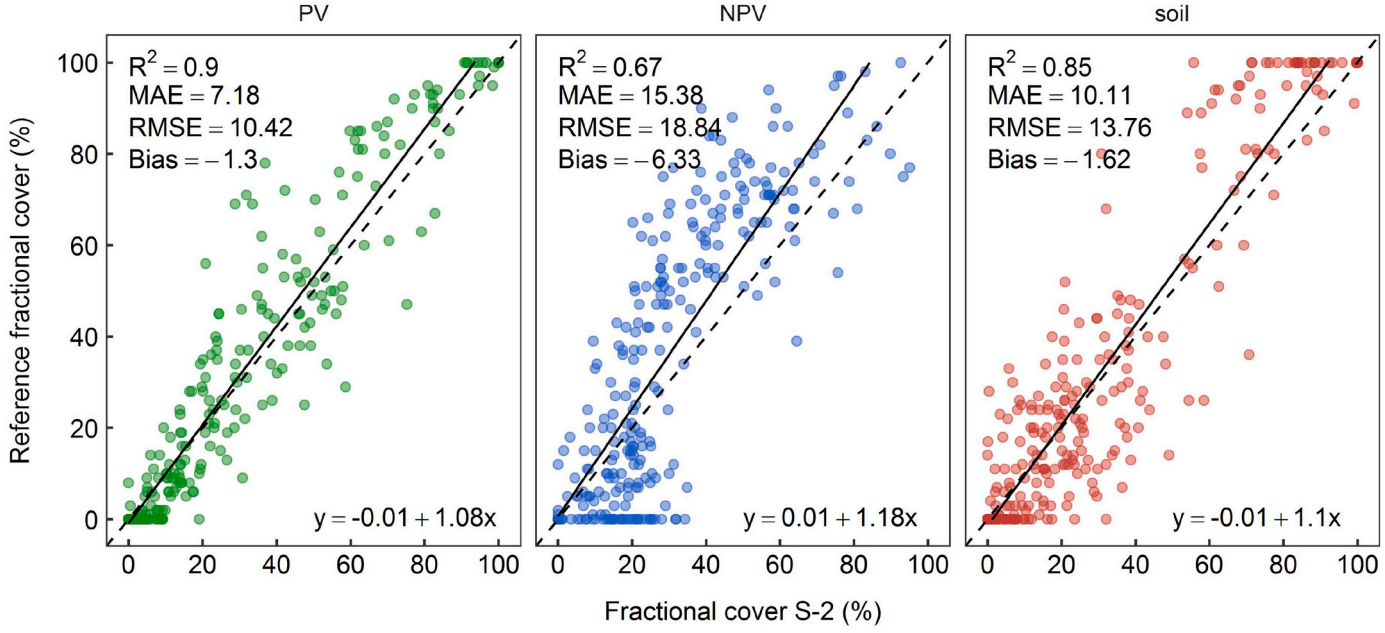

Fig. 6. Comparison of PV, NPV, and soil fractional cover from Sentinel-2 and reference fractional cover from VHR imagery.

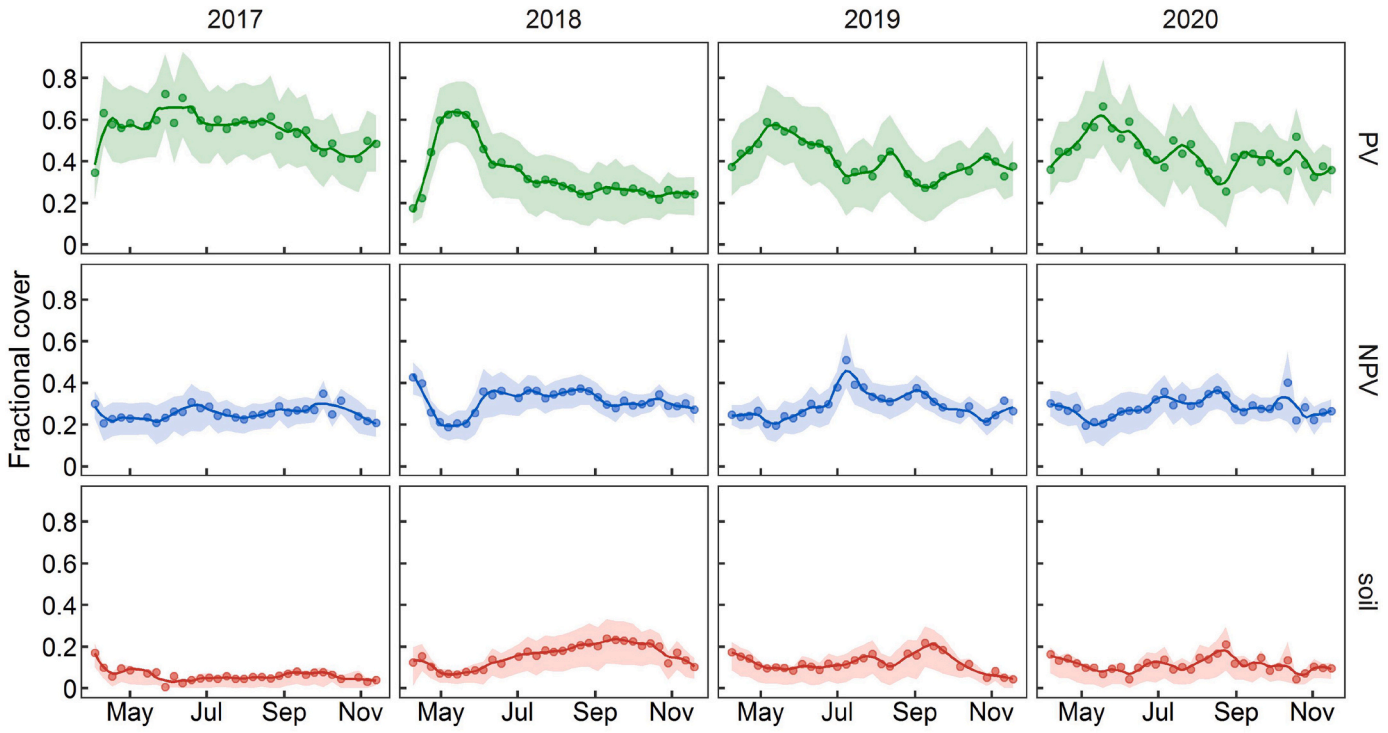

Fig. 7. Weekly averages of PV, NPV, and soil fractional cover from Sentinel-2 (2017–2020) for the complete study area. Shading around the mean values indicate the 25th and 75th percentiles.

slightly lower than in 2018. Still, more than half of the grassland area had high NPV and soil fractions from July to September. In 2020, NPV and soil cover were overall less dominating than in 2018 and 2019, indicating recovery of the grassland vegetation. In August, half of the grasslands had high NPV and soil cover, similar to the previous year.

The seasonal development of the NDFI and NDVI were very similar. Yet, the NDFI provided a higher degree of differentiation of grassland conditions. This became especially evident in the drier summer months of 2018, 2019 and 2020 when grassland vegetation changed from high PV to high NPV and soil fractional cover (Fig. 9a, b). Within these months, fractional cover-based NDFI values stretched across the whole value range from −1 to 1, allowing an optimized differentiation of drought-related processes, whereas NDVI values were mostly constrained to the range of 0.4 to 0.85.

The high drought impact on grassland vegetation in 2018, 2019, and partly 2020 was corroborated by the distributions of the meteorological drought indices and the SMI (Fig. 9c, d, e). All indices showed the most severe precipitation and soil moisture deficits in 2018, followed by 2019 and 2020, whereas 2017 was characterized by average precipitation and soil moisture. SPI03, SPEI03 and SMI values below their respective thresholds indicate the beginning of the drought in May 2018. From NDFI time series, the effects on the majority of grasslands become apparent in June and July 2018, suggesting a time lag of precipitation and soil moisture deficit effects on grasslands of 1–2 months. SPI03, SPEI03 and SMI showed that growing conditions did not improve considerably during early spring 2019. For 2020, SPI, SPEI, and SMI suggested slightly improved growing conditions compared to the previous two years, but the indices were below their respective thresholds for most months in 2020 indicating a mild to moderate drought. Slight improvements of growing conditions were in line with the NDFI indicating dominating PV cover in all months for most grasslands, except for August when ca. 50% of grasslands had higher NPV and soil cover again. Interestingly, the SPI03 showed less severe drought conditions from 2018 to 2020 compared to the SPEI03 and SMI, suggesting that temperature had a strong impact on drought severity captured by SPEI03 and SMI. Compared to the NDFI, both meteorological indices and the SMI exhibited considerably lower spatial variations across the study area during the drought years of 2018 and 2019.

4.4. NDFI-based drought metrics

Investigating drought-specific metrics of the longest period of NDFI >0, we again found differences between but also within the three growing seasons. The season of 2017 was characterized by short-time increases of NPV and soil cover relative to PV cover (Fig. 10b) for ca. 60% of the grasslands. The timing of these cover changes was distributed across the growing season with the strongest increase in early September (Fig. 10a). Combined with the short duration of cover changes, this indicates that high NPV or soil cover occurred during short time management events within the season or during senescence in autumn. For the remaining 40% of the grasslands, no time period of NDFI >0 was found within the growing season suggesting high PV cover from April to mid-November. For 2018, we found the overall longest and most severe drought impacts in the study period. For example, seasonal NPV and soil cover persisted for a minimum of three months within the growing season on nearly 50% of all grasslands (Fig. 10b). In 2019 and 2020, this was the case for 25% and 15% of all grasslands, respectively, showing continuously shorter time periods of high NPV and soil cover. For 2018, 2019, and 2020, the onset of high NPV and soil cover was concurrent with the strongest increase (ca. 50% of grasslands) from the end of May until mid-July (Fig. 10a).

We found a high variability of metrics within and between grassland sites (Fig. 10). For example, the duration of high NPV and soil cover fractions differed considerably within and across grassland parcels during 2018 and 2019, where spatial patterns indicated differences that may relate to soil type, species composition or grassland management (Fig. 10b). The beginning and end of high NPV and soil cover in 2017 aligned well with the shapes of individual grassland parcels, suggesting that high NPV and soil cover in 2017 was mostly driven by grassland management (Fig. 10a, d). From 2018 to 2020, different field patterns

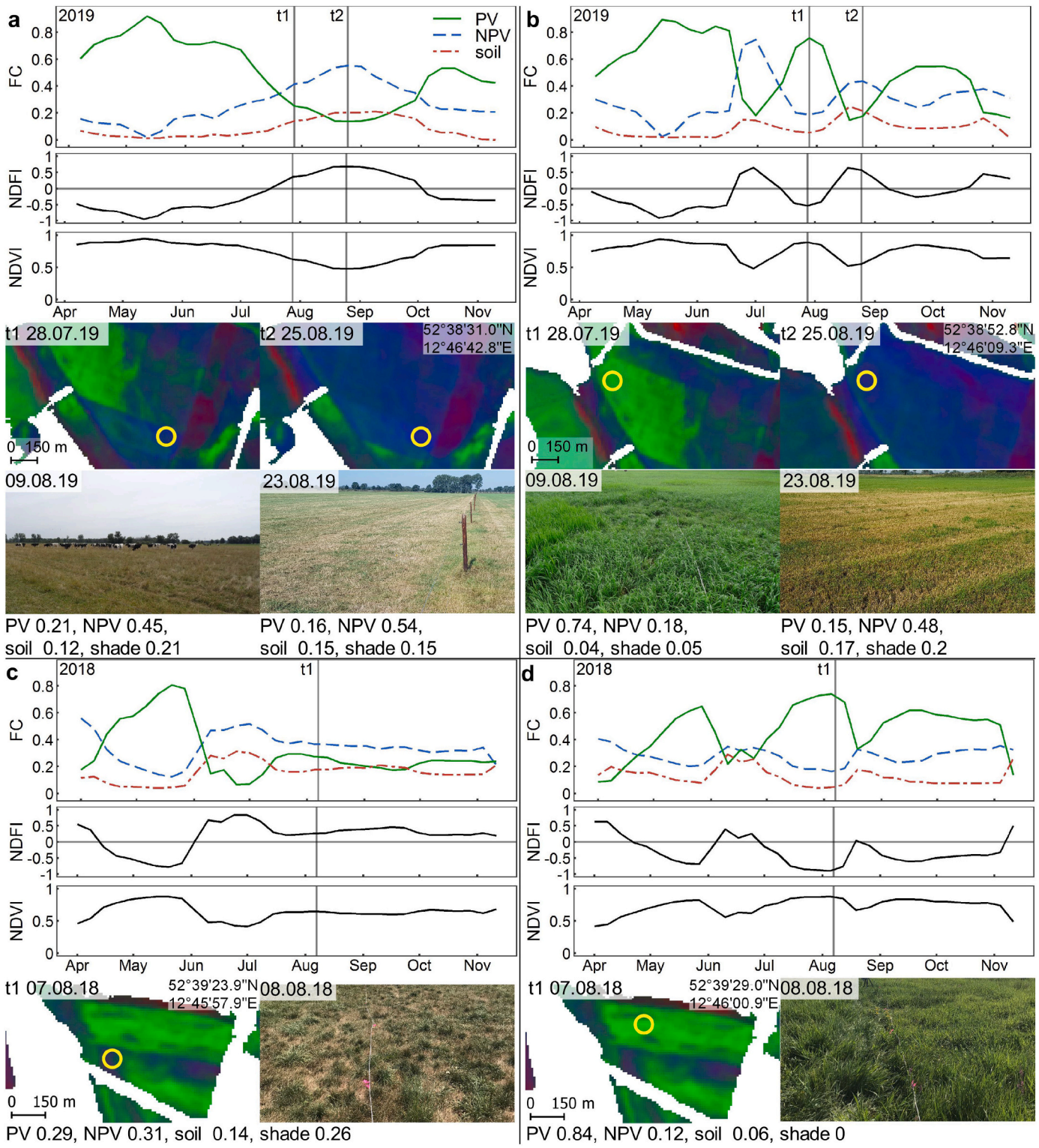

Fig. 8. Time series of PV, NPV, and soil fractional cover, NDFI, and NDVI from Sentinel-2 for different field sites (a-d). Sentinel-2 fractional cover and corresponding images show in-situ conditions. Field sites relating to the time series and images are marked with yellow circles. (For interpretation of the references to colour in this figure legend, the reader is referred to the web version of this article.)

were still evident but both metrics were more homogenously distributed across different fields, especially during the most severe drought in 2018. For grasslands in Fig. 10c, a strong East-West gradient of the fractional cover changes was evident in 2018 whereas this gradient was less apparent in 2017 and became weaker in 2019 and 2020.

Combining the duration and magnitude (i.e., mean NDFI during NDFI >0) of high NPV and soil cover into a bivariate map (Fig. 11 for 2018, Fig. S1, Fig. S2, and Fig. S3 for 2017, 2019, and 2020, respectively. The maps are available via an interactive web viewer: https://ows.geo.hu-berlin.de/webviewer/grassland_drought/) enabled identifying different fractional cover dynamics within a season: Short periods of high NPV and soil cover with highest mean NDFI appear in bright

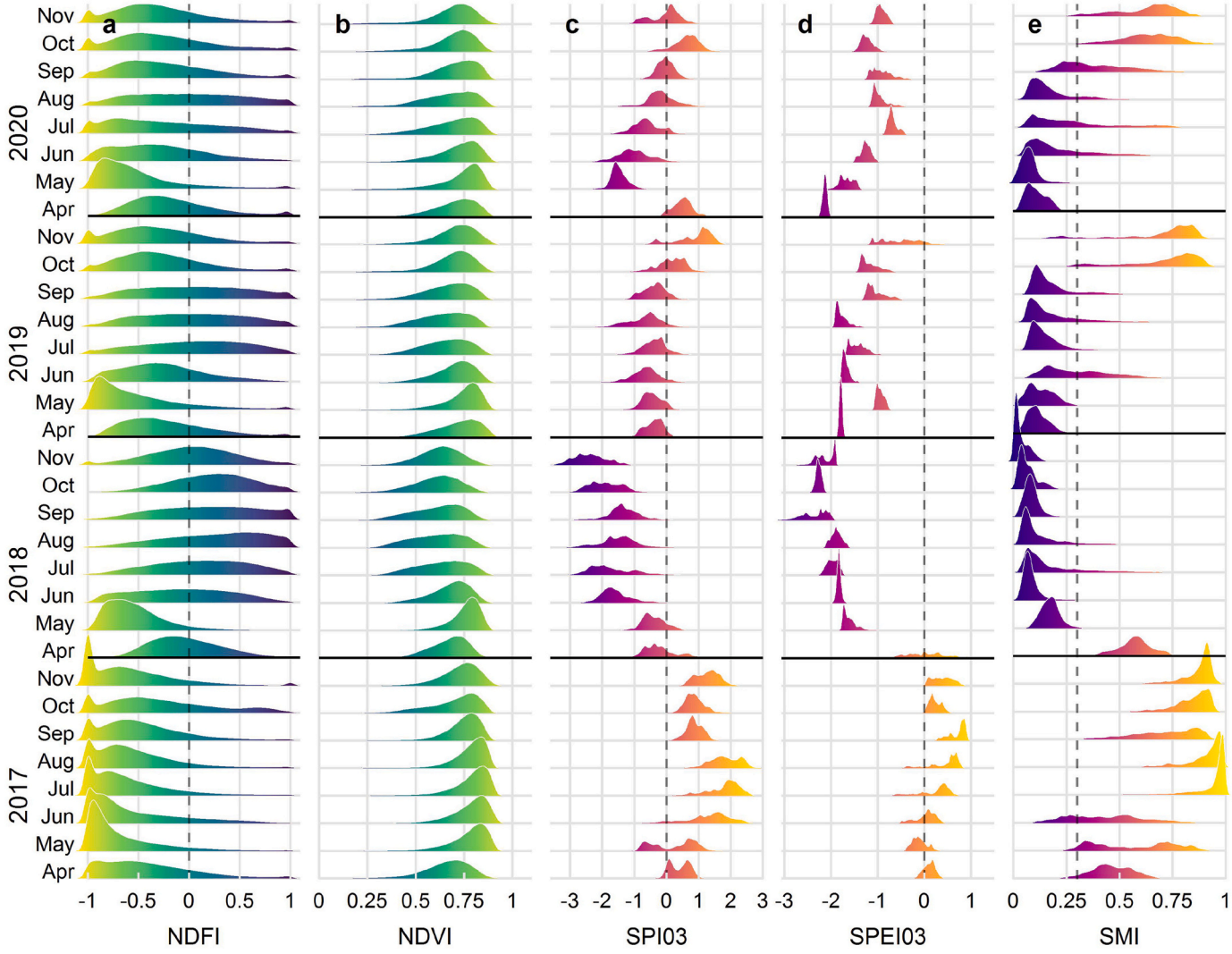

Fig. 9. Monthly density distributions of NDFI, NDVI, SPI03, SPEI03, and SMI from 2017 to 2020. NDFI values above 0 indicate higher NPV and soil cover in relation to PV cover. For SPI03 and SPEI03, negative values denote increasingly dry conditions. SMI values below 0.3 indicate abnormally dry conditions. Note that the density scaling is different for each index.

blue, whereas the longest-lasting changes with a low mean NDFI appear in yellow. The most striking drought impacts, with high and long-lasting NPV and soil cover fractions dominating are colored in magenta. The maps reveal spatial clusters of similar grassland cover dynamics across the study area within each growing season. We observed that these clusters were located on different soil types. For example, large coherent grassland areas on fen soils (Histosols) in the northeastern part of the study area were characterized by mainly short and moderately high NPV and soil cover during 2018 (Fig. 11b, c, central part in Fig. 11f). We abundantly found similar dynamics across the entire study area when grasslands were located on Histosols (Fig. S4). Compared to other soil types, grasslands on Histosols experienced the weakest (mean NPV and soil cover of 64–67%) and shortest (41–62 days) drought impacts in 2018 and 2019 (Table 1). In contrast, we found more severe and long drought effects on grasslands on sandy Cambisols (e.g., Fig. 11g, Table 1). Similarly, grasslands on Fluvisols along the Elbe river near the western border of the study area (Fig. 11a) were covered by high percentages of NPV and soil (66–73%) for most of the growing season of 2018 and 2019 (Table 1). Grasslands on these soils showed the strongest decrease in both duration and mean NDFI in 2020 (Fig. S3a), indicating improving growing conditions. Although drought impacts differed between the soil types, we observed substantially higher NPV and soil cover (9–18% increase) with a longer duration (26–104 days longer) in 2018 and 2019 compared to 2017 on all soil types. This corroborates the high impacts of the continuing drought event on all grasslands. In 2020, the duration of high NPV and soil cover decreased substantially by 29–74 days and 8–31 days compared to 2018 and 2019, respectively. Similarly, average NPV and soil cover was up to 11% lower in 2020 than in the previous two years, indicating recovery of grassland growth after the severe drought in 2018 and 2019.

5. Discussion

5.1. PV, NPV, and soil fractional cover time series from Sentinel-2

Comparing the fractional cover from multispectral Sentinel-2 data to a multitemporal reference dataset based on interpretation of VHR imagery, we found that Sentinel-2 is well suited to derive fractional cover of PV, NPV, and soil in our study area. PV cover agreed best with the reference data. Our results confirm previous studies showing that multispectral data, and in particular Sentinel-2, are well suited for mapping the PV fraction accurately (e.g. Corbane et al., 2014; Guerschman et al., 2015; Ji et al., 2020). Using PV fractional cover reduces saturation effects (Gitelson et al., 2002) as well as sensitivity deficiencies under drought (Xu et al., 2014). For NPV and soil, we observed higher uncertainties than for PV. Over- and underestimations of soil and NPV in

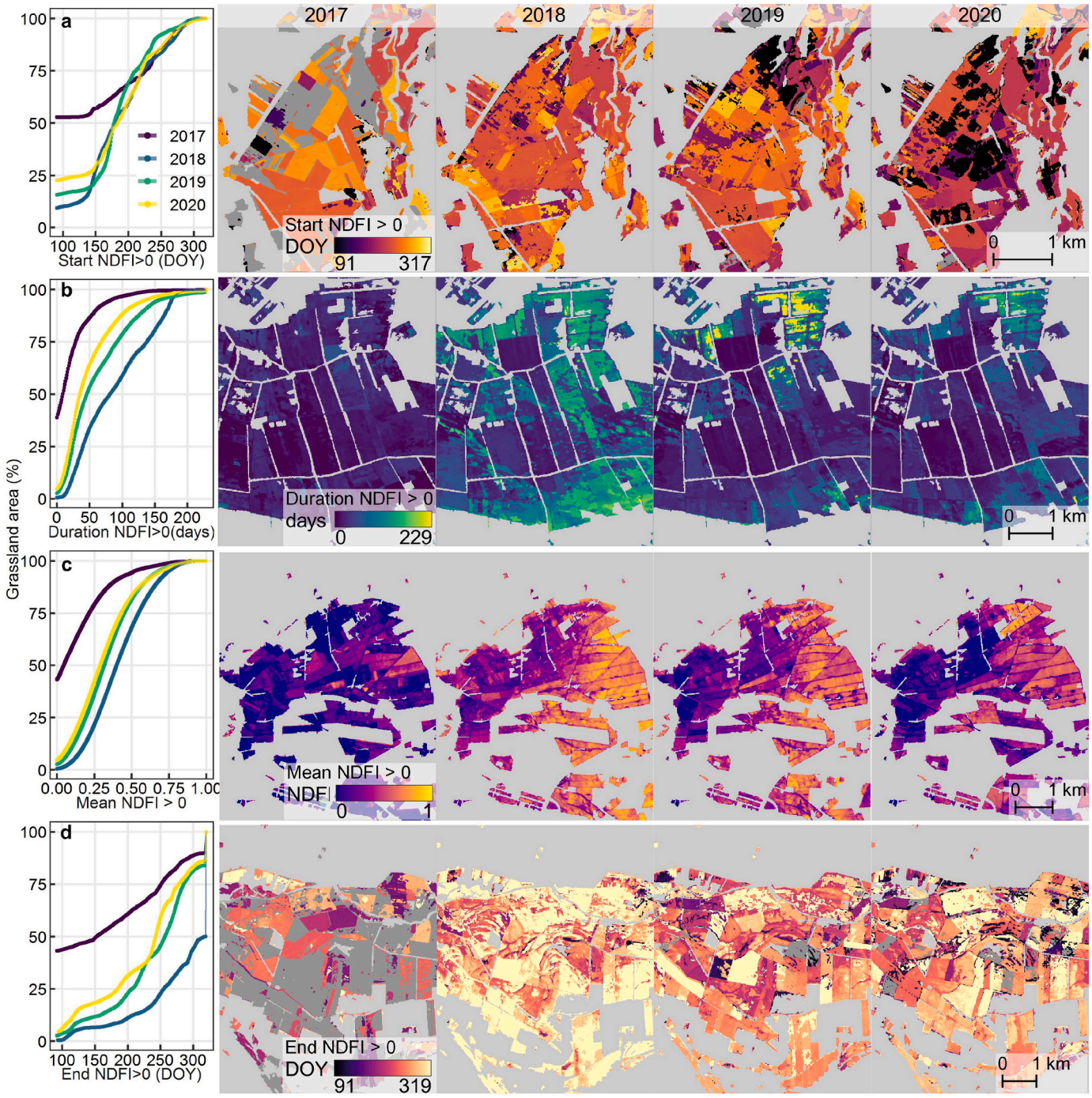

Fig. 10. Cumulative distribution of drought metrics based on NDFI time series across the study area (left column) and examples of different grassland sites for each growing season (dark grey areas correspond to pixels with no time period of NDFI >0).

low and high value ranges, respectively, indicated a slight confusion of these cover types. Estimating NPV and soil fractional cover from multispectral data is generally challenging due to the spectral similarity between the two classes (Asner and Heidebrecht, 2002). Regarding the spectral configuration of Sentinel-2, two aspects are important for estimating NPV and soil fractional cover: First, Sentinel-2 spectral bands do not capture the cellulose and lignin absorption of NPV in the shortwave infrared directly, while this spectral absorption feature at 2100 nm has been frequently used to differentiate NPV and soil cover from hyperspectral data (Asner and Heidebrecht, 2002). However, similar to Guerschman et al. (2009), we found that NPV typically has a considerably lower reflectance than soil in the SWIR band centered on 2200 nm, increasing the spectral separability of NPV and soil for our study area. Second, results by Ji et al. (2020) and Tian et al. (2021) suggest, that the three red-edge bands and the relatively narrow NIR band of Sentinel-2 provide additional information for separating NPV from soil. NPV often exhibits a stronger reflectance increase in the red-edge wavelength region towards the NIR than soils. However, this increase also varies with decomposition status of NPV and soil moisture (Nagler et al., 2000). Such variations partly explain the confusion of soil and NPV from our models as managed, temperate grasslands in Central Europe often exhibit a thin layer of litter with different decomposition stages depending on the management type (Sanaullah et al., 2010).

Photographs from field visits on multiple dates corroborated that the

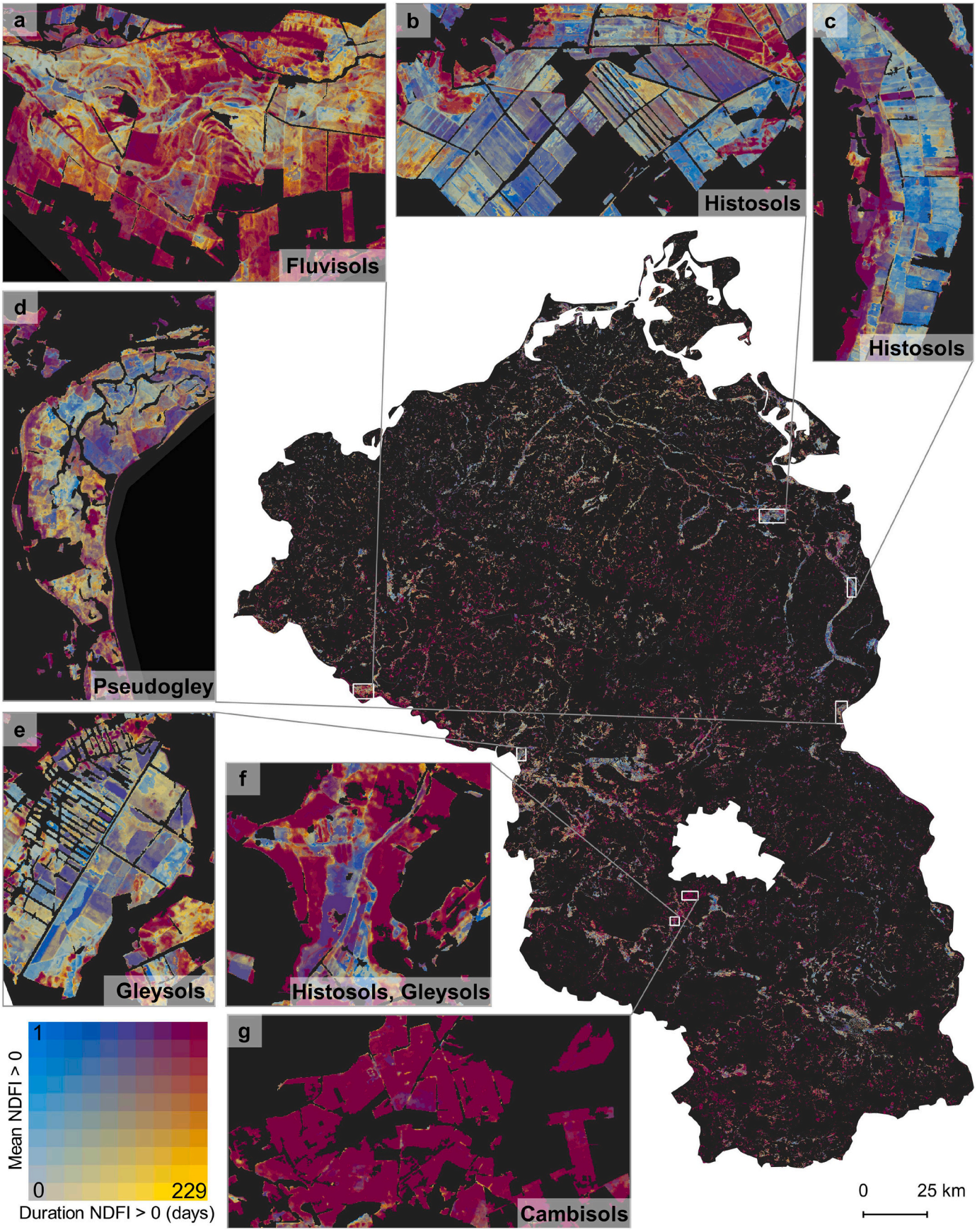

Fig. 11. Bivariate map of the duration and mean NDFI based on the longest time period when NDFI >0 for the growing season 2018. Values were binned into deciles.

Table 1
Averages of seasonal drought metrics (mean NDFI and duration) for different soil types in the study area according to Fig. S4. We excluded soil types summing up to less than 1% of the total grassland area (Regosols, Podzols, Chernozems).

		Mean NDFI > 0 (% NPV/soil)				Duration in days			
Soil type	Grassland area (%)	2017	2018	2019	2020	2017	2018	2019	2020
Cambisols	20.26	0.16 (58%)	0.49 (75%)	0.40 (70%)	0.35 (69%)	29	116	90	70
Fluvisols	4.39	0.10 (55%)	0.45 (73%)	0.33 (66%)	0.24 (62%)	12	116	73	42
Gleysols	24.8	0.13 (57%)	0.42 (71%)	0.33 (67%)	0.30 (65%)	21	95	64	48
Histosols	30.1	0.11 (55%)	0.34 (67%)	0.27 (64%)	0.26 (63%)	15	62	41	33
Luvisols	5.54	0.14 (57%)	0.44 (72%)	0.36 (68%)	0.35 (68%)	22	97	66	57
Podzoluvisols	2.39	0.17 (59%)	0.49 (74%)	0.41 (70%)	0.40 (70%)	27	111	80	66
Pseudogley	6.81	0.14 (57%)	0.38 (69%)	0.32 (66%)	0.31 (66%)	22	84	55	47

fractional cover time series tracked in-situ grassland conditions during management events and drought. The reference dataset based on VHR images facilitated a temporally and spatially detailed validation of fractional cover time series. While available VHR images provide detailed reference information, very fine-scale features, e.g., single plant leaves and soil under a thin layer of litter, were not always clearly discernible. This likely contributed to deviations of NPV and soil fractional cover derived from Sentinel-2 in low value ranges. Still, the cm-resolution images allowed for identifying the dominant cover type of PV, NPV, or soil on a 1 × 1 m scale based on colour, structural and contextual information.

This study demonstrates the opportunities provided by the Sentinel-2 mission for retrieving fractional cover time series for grassland ecosystems. Our findings from a Central European region complement similar studies based in other regions or on other sensors (e.g., Guerschman et al., 2009; Lewińska et al., 2020). The trajectory of PV fractional cover represented the expected seasonal phenology well within individual years, with highest growth rates, i.e., increase in PV fractions in late spring to early summer, and growth cessation, i.e., decrease in PV fractions, in late summer to autumn with decreasing photoperiod and beginning cold acclimation at temperatures of 5–10 °C (Wingler and Hennessy, 2016). This seasonal variation was shown to be altered by other factors, including meteorological variability, i.e., droughts or extreme rainfall (Chang et al., 2017; Cremonese et al., 2017) and land management (Wingate et al., 2015). In this context, the trajectories of NPV and soil fractional cover provided additional thematically relevant information, e.g., increasing average NPV and soil cover during the drier years in 2018 and 2019 compared to the pluvial season of 2017 indicating the value of both quantities for drought assessment. This is in line with Meyer and Okin (2015) and Numata et al. (2007) who emphasize the use of NPV fractions for monitoring savannas and grasslands, respectively, during the dry seasons. In our study area, the high spatial heterogeneity of fractional cover time series between and within individual grassland plots pointed to differences in land use intensity but also soil characteristics (Fig. 8). In this regard, it is obvious that the spatial resolution of Sentinel-2 is especially relevant to capture such spatial details.

5.2. Seasonal drought impacts on grasslands based on NDFI time series

We introduced a normalized fraction index based on proportions of NPV and soil relative to PV cover to emphasize the use of our fractional cover time series for drought effect assessment in Central European grasslands. We found extended time periods with high NPV and soil cover during the growing seasons of 2018 and 2019, indicating that the majority of grasslands was not resistant to the persisting drought. This is not surprising as the growing season of 2018 was characterized by the highest temperatures combined with lowest precipitation recorded in Germany since 1881 (Zscheischler and Fischer, 2020). Similar, but less severe conditions persisted during the growing season of 2019 (Hari et al., 2020) and 2020 (German Weather Service, 2020), when we observed shorter and weaker NPV and soil cover increases.

SPI03, SPEI03 and SMI indicated similar dynamics between the four years. However, based on the high-resolution fractional cover time series from Sentinel-2 we found a high variation of vegetation response to drought across the study area for 2018 and 2019. In comparison, SPI03, SPEI03, and SMI did not show such a high variability in these years. These differences can be expected, as meteorological droughts captured by SPI and SPEI are controlled by large-scale atmospheric circulation patterns leading to homogenous drought conditions in our study region in 2018 (Drouard et al., 2019; López-Moreno and Vicente-Serrano, 2008). The process-based mesoscale Hydrological Model (mHM) is also forced with meteorological variables. Additionally, topography, soil texture, and land cover data are included in the model (Samaniego et al., 2010). However, the resulting SMI is available on a resolution of 4 km only, which likely contributed to the lower variability compared to the NDFI. Drought effects on grassland cover vary locally with management intensity (Zwicke et al., 2013), soil characteristics (e.g. organic matter content (Buttler et al., 2019)) and drought resistance of plant species (Mariotte et al., 2013). It is not possible to analyze these local-scale differences with purely meteorological information of SPI03 and SPEI03, or with the SMI on 4 km spatial resolution. Analyzing spatially aggregated drought indices such as SPI, SPEI, and SMI together with the fractional cover-based NDFI now allows for a more nuanced, local-scale evaluation of vegetation changes during drought periods.

The NDFI showed overall similar seasonal patterns as the NDVI within the four growing seasons. The seasonal dynamics observed from both indices are in line with the findings by Reinermann et al. (2019), who also identified the first negative deviations in June 2018 based on the EVI. Different from NDVI and other greenness-based indices, NDFI is based on percent cover of PV, NPV, and soil in grasslands. Thereby, the NDFI allows for an intuitive interpretation and thresholding, which is not possible when using NDVI alone without ancillary data or long time series. Apart from vegetation indices, other biophysical measures (e.g., Leaf Area Index (LAI) and aboveground biomass (AGB)) have been used to analyze drought impacts on grassland vegetation (e.g., Li et al., 2018; Mariano et al., 2018). Grassland-specific LAI and AGB estimates usually rely on extensive field databases, which often limit their application for larger areas and across time series (Ali et al., 2016). Compared to fractional cover, senescent grassland vegetation is usually not accounted for in AGB or LAI estimations (Delegido et al., 2015; Schwieder et al., 2020; J. Wang et al., 2019a), even that recent findings indicate potential of using LAI-based models for differentiating PV and NPV in croplands based on Sentinel-2 data (Amin et al., 2021). Deriving quantitative estimates of non-photosynthetically active and photosynthetically active plant materials is, however, important for analyzing grassland vegetation during drought periods (Coates et al., 2015; Guerschman et al., 2020). The adapted version of the NDFI presented in this study quantifies NPV changes within each season by correcting for pre-season NPV cover (e.g., from previous years). Thus, the resulting NDFI and corresponding fractional cover values can be interpreted as the seasonal increase of NPV and soil during drought periods. Overall, the fractional

cover-based NDFI is accordingly a promising approach for quantifying the grassland response to drought based on a physically meaningful measure.

5.3. Spatial patterns of grassland drought

We found a high spatial variability of the drought response of grasslands associated with different soil types. Almost a third of all grasslands in the study area are located on peat soils (Histosols) where grassland vegetation was less severely affected by drought compared to other soil types. These peatlands have been drained in the past to make the land available for grassland cultivation (Landesamt für Ländliche Entwicklung, Landwirtschaft und Flurneuordnung (LELF), 2014; Landesumweltamt Brandenburg (LUA), 2004). Grasslands likely benefited from groundwater resources during the drought in 2018 and 2019, which usually respond with a time lag of several months to drought (Hellwig et al., 2020). Moreover, the high soil organic matter content of Histosols and Gleysols contributes to a higher drought resistance (Buttler et al., 2019). Yet, future drought impacts might be alleviated by permanently increasing water levels on such grasslands. This would not only enhance their drought resistance but also mitigate the substantial greenhouse gas emissions, submergence, and soil degradation of drained peatlands (Tanneberger et al., 2020). However, it is still unclear how and if rewetting of former peatlands can be harmonized with the needs of land users (e.g., fodder production for dairy/cattle farming) and current fauna and flora conservation goals (Buschmann et al., 2020). Conversely, grasslands on Cambisols were strongly impacted by drought conditions in 2018 and 2019. Grasslands on these soil types were already characterized by slightly higher shares of NPV and soil cover compared to other grasslands in the wet year of 2017. These vegetation dynamics suggest a low productivity under pluvial growing conditions. The observed differences to other soil types were further amplified during the drought in 2018 and 2019. As the temperate grasslands of Central Europe are mostly located on poorer sites, which are not suitable for cropping, a lower water holding capacity and low soil organic matter content of Cambisols can explain the stronger drought impacts on these grasslands. More frequent droughts in the future will likely exacerbate the observed differences with highest drought impacts on less productive grassland sites.

The drought response of grasslands is modulated by a variety of factors (e.g., abiotic growing conditions, soil characteristics, land management, functional groups of grassland species) and their local interactions (De Boeck et al., 2011; Vogel et al., 2012; Wellstein et al., 2017). For example, grasslands in Fig. 10b are growing on drained fen soils with varying soil organic matter content and groundwater levels. Such growing conditions cause different species compositions (Kaiser et al., 2001; Schwieder et al., 2020) and therefore heterogeneous drought impacts on grassland vegetation on fine spatial scales. Grasslands in Fig. 10d were an example of the strong influence of varying groundwater levels on grassland vegetation during drought periods. The East-West gradient in the drought impact was related to the close-by (ca. 2 km distance) open-pit lignite mine, which requires permanent lowering of the groundwater level around the mine (Grünewald, 2001). While this is not a typical setting for grasslands in Central Europe, it confirms the high impact of local water management on grassland vegetation during droughts. Overall, these findings indicate that hydrological processes play a major role in determining the vegetation development during droughts. More detailed information on hydrological processes should therefore be used in future studies together with remote sensing-based estimates of drought effects to gain a better understanding of grasslands' response to droughts.

For 40% of the grassland area, no period of NDFI >0 was identified in 2017. While the other three years were characterized by overall warmer and drier conditions, high NPV and soil cover should still be observable after management events in 2017, which was rarely the case. Such short-term disturbances of the grassland vegetation were likely missed in the NDFI time series due to the lower observation frequency in 2017 (Fig. S5). Griffiths et al. (2020) also noted that less cloud-free observations likely led to the omission of mowing events in their detection algorithm which was applied across Germany. The seasonal metrics derived for 2017 should therefore be interpreted with caution. Overall, the NDFI time series and metrics derived thereof still showed the expected seasonal patterns in line with the meteorological drought indices and SMI which were not influenced by cloud cover. The season of 2017 was an exception with high cloud cover and incomplete Sentinel-2B acquisitions until summer. However, cloud-free observation frequencies similar to 2017 still occurred outside swath overlap areas in all other years. The variations of cloud-free observations within and between years consequently require further research, as the number of valid observations can affect time series metrics, which has already been shown for our study area (Kowalski et al., 2020).

5.4. Transferability of regression-based unmixing for drought analysis

We presented a framework for estimating grassland fractional cover time series in a Central European grassland region based on Sentinel-2 data. Within this framework, a spectral library for generating synthetic training data for subsequent regression-based unmixing was constructed. To ensure consistent and comparable PV, NPV, and soil cover estimates through time, we selected a global set of library spectra representative of the entire time series based on the triangular NDVI/SWIR ratio feature space from 4 years of Sentinel-2 data. We followed the common approach to choose one representative spectral signature for each cover class (e.g., Lewińska et al., 2020; Röder et al., 2008) from the vertices of the feature space (Guerschman et al., 2009; G. Wang et al., 2019a). The position of the library spectra relative to the overall shape of the feature space throughout the time series showed that the selected spectra were representative for grasslands in our study area from 2017 to 2020.

Transferring this approach to other grassland ecosystems requires insights into the spectral variability of cover types in the target region. The spectral variability is related to different vegetation structures, soil characteristics, and topography. While topographic illumination differences in mountainous regions can be accounted for with rigorous preprocessing (Buchner et al., 2020), different species compositions, soil colors and changing moisture contents can change the shape of PV, soil and NPV reflectance spectra and thus the shape of the feature space (Daughtry and Hunt, 2008; Lopatin et al., 2017). For the case that pure spectra of PV, NPV, and soil form a similar triangular NDVI/SWIR ratio feature space in other grassland ecosystems, separation between these cover types should be possible and we assume that our framework can be transferred based on adapted or region-specific spectral libraries. In fact, the concept of the NDVI/SWIR ratio feature space for quantifying PV, NPV, and soil fractional cover was developed in Australian savanna ecosystems (Guerschman et al., 2009) and our study therefore represents a successful case for a transfer of the approach. However, distinguishing NPV from soil with multispectral data is very critical in many regions (Guerschman et al., 2015). In case that pure NPV and soil are spectrally too similar and thus do not form a triangular feature space, it is likely that the framework cannot be transferred. Hill et al. (2016) and Hill et al. (2017) estimated PV, NPV, and soil fractional cover in two savanna ecosystems in southern Africa and Brazil, respectively. Their results suggested high uncertainties for estimating NPV and soil fractional cover in heterogenous vegetation types with a complex phenology. Uncertainties of separating NPV and soil also relate to the limited information content of multispectral data. In this regard, data from forthcoming spaceborne hyperspectral missions (e.g., CHIME (Nieke and Rast, 2018) and SBG (Green, 2018)) have a high potential for more precise estimates with a continuous global coverage. Compared to structurally complex ecosystems such as savannas, the vegetation structure of most grasslands in Central Europe is comparably homogenous without any considerable shrub or tree cover (Hejcman et al.,

2013). Overall, we therefore expect that the framework is transferable to similar Central European grasslands, while detailed analyses of spectral variance are needed in regions where soils, topography and climate are inherently different.

We developed our approach based on all available Sentinel-2 data from four years. By including all seasons with combined Sentinel-2A/B data, we covered extreme as well as average growing conditions. Compared to other multispectral sensors used for estimating fractional cover time series, Sentinel-2 offers improved spectral and spatial resolution which captured grassland vegetation dynamics with high detail. However, fractional cover time series from Sentinel-2 are limited to recent years. Analyses of historic time series and respective deviations of intra-annual observations are crucial to gain a better understanding of recent drought impacts in comparison to past decades. The vegetation condition index (VCI) has been widely used for this purpose, as it compares the observed NDVI value to the long-term minima and maxima during the same time period (Ji and Peters, 2003; Kogan, 1995). Generalizing the regression-based unmixing approach across sensors, e.g., by making regression models transferable through the Landsat archive would enable time series analyses including data from more than three decades (Wulder et al., 2016). However, compared to Sentinel-2, Landsat has a considerably lower observation frequency. Sparse time series require modified approaches such as pooling observations from several years (Melaas et al., 2013; Senf et al., 2017) or annual cumulative fractional cover estimates (Lewińska et al., 2020). Detailed intra-annual analyses of grassland time series are thus limited to recent years with Sentinel-2 data. Moreover, Landsat's lower spatial resolution of 30 m and the lower spectral information can lead to higher uncertainties for fractional cover estimation (Ji et al., 2020). Yet, PV, NPV, and soil fractional cover have been derived from Landsat for grasslands (Guerschman et al., 2015; He et al., 2020; Yu et al., 2019) indicating potential for using Landsat time series in Central European grasslands as well.

6. Conclusions

In this study, we presented an approach for quantifying drought effects in a major Central European grassland region. The approach includes (i) the derivation of intra-annual PV, NPV, and soil fractional cover time series using all available Sentinel-2 data between 2017 and 2020 and regression-based unmixing, and (ii) the calculation of the NDFI, an index to emphasize the use of our fractional cover time series for drought effect assessment. Validation based on multitemporal reference information from VHR imagery revealed that PV, NPV, and soil fractions were effectively estimated in our study site, while the NDFI calculated thereof proved to track the strongest drought impacts in 2018 and 2019. Yet, grasslands responded non-uniformly to the severe drought and heatwave within each season. Differences were related to soil types and varying growing conditions within and between grassland parcels. Consequently, compatible in-situ data are needed to deepen a process-based understanding of the complex drought responses of grasslands to diverse environmental conditions and management. Future experiments should be distributed across grassland drought impact gradients – knowledge that is only derivable in space and time based on detailed and quantitative maps from satellite remote sensing.

Our study showed that high spatial and temporal resolution satellite remote sensing data are mandatory to monitor grassland dynamics during drought periods. To date, Sentinel-2 provides the only freely available data with sufficient spatial and temporal resolution. Given the universality of our methodological framework, we are convinced that our approach constitutes a useful means for drought impact assessment in Central European grassland systems from Sentinel-2 data in general. Therefore, future research should focus on transferring the approach to ecologically different Central European grassland systems.

Declaration of Competing Interest

The authors declare that they have no known competing financial interests or personal relationships that could have appeared to influence the work reported in this paper.

Acknowledgements

This research was funded within the frame of “GreenGrass” (Federal Ministry of Education and Research, Germany (BMBF), grant number: 031B0734I). The project “SOIL-DE” (Federal Ministry of Food and Agriculture (BMEL), grant number: 281B301716) provided the soil type map. We thank two anonymous reviewers for their helpful suggestions to improve this study. We thank David Frantz for facilitating data processing in FORCE and Clemens Jänicke for providing the code for the meteorological drought indices. We also thank Marcel Schwieder and Lukas Blickensdörfer for providing the land use map.

Appendix A. Supplementary data

Supplementary data to this article can be found online at https://doi.org/10.1016/j.rse.2021.112781.

References

Adams, J.B., Smith, M.O., Johnson, P.E., 1986. Spectral mixture modeling: a new analysis of rock and soil types at the Viking Lander 1 Site. J. Geophys. Res. 91, 8098. https://doi.org/10.1029/JB091iB08p08098.

Ali, I., Cawkwell, F., Dwyer, E., Barrett, B., Green, S., 2016. Satellite remote sensing of grasslands: from observation to management. JPECOL 9, 649–671. https://doi.org/10.1093/jpe/rtw005.

Ali, I., Cawkwell, F., Dwyer, E., Green, S., 2017. Modeling managed grassland biomass estimation by using multitemporal remote sensing data—a machine learning approach. IEEE J. Select. Top. Appl. Earth Observ. Remote Sens. 10, 3254–3264. https://doi.org/10.1109/JSTARS.2016.2561618.

Amin, E., Verrelst, J., Rivera-Caicedo, J.P., Pipia, L., Ruiz-Verdú, A., Moreno, J., 2021. Prototyping Sentinel-2 green LAI and brown LAI products for cropland monitoring. Remote Sens. Environ. 255, 112168. https://doi.org/10.1016/j.rse.2020.112168.

Amt für Statistik Berlin-Brandenburg, 2019. Statistischer Bericht - Ernteberichterstattung über Feldfrüchte und Grünland im Land Brandenburg 2018. Potsdam, Germany.

Asner, G.P., Heidebrecht, K.B., 2002. Spectral unmixing of vegetation, soil and dry carbon cover in arid regions: comparing multispectral and hyperspectral observations. Int. J. Remote Sens. 23, 3939–3958. https://doi.org/10.1080/01431160110115960.

Awad, M., Khanna, R., 2015. Support vector regression. In: Efficient Learning Machines. Apress, Berkeley, CA, pp. 67–80. https://doi.org/10.1007/978-1-4302-5990-9_4.

Bahn, M., Ingrisch, J., Jentsch, A., 2019. Grünlandnutzung. In: Wohlgemuth, T., Jentsch, A., Seidl, R. (Eds.), Störungsökologie. UTB, Stuttgart, pp. 304–324.

Bannari, A., Morin, D., Bonn, F., Huete, A.R., 1995. A review of vegetation indices. Remote Sens. Rev. 13, 95–120. https://doi.org/10.1080/02757259509532298.

Barnett, K.L., Facey, S.L., 2016. Grasslands, invertebrates, and precipitation: a review of the effects of climate change. Front. Plant Sci. 7 https://doi.org/10.3389/fpls.2016.01196.

Bayat, B., Van der Tol, C., Verhoef, W., 2016. Remote sensing of grass response to drought stress using spectroscopic techniques and canopy reflectance model inversion. Remote Sens. 8, 557. https://doi.org/10.3390/rs8070557.

Beierkuhnlein, C., Thiel, D., Jentsch, A., Willner, E., Kreyling, J., 2011. Ecotypes of European grass species respond differently to warming and extreme drought. J. Ecol. 99, 703–713.

Bengtsson, J., Bullock, J.M., Egoh, B., Everson, C., Everson, T., O'Connor, T., O'Farrell, P. J., Smith, H.G., Lindborg, R., 2019. Grasslands—more important for ecosystem services than you might think. Ecosphere 10, e02582. https://doi.org/10.1002/ecs2.2582.

Blickensdörfer, L., Schwieder, M., Pflugmacher, D., Nendel, C., Erasmi, S., Hostert, P., 2021. National-scale crop type maps for Germany from combined time series of Sentinel-1, Sentinel-2 and Landsat 8 data (2017, 2018 and 2019). https://doi.org/10.5281/ZENODO.5153047.

Bolton, D.K., Gray, J.M., Melaas, E.K., Moon, M., Eklundh, L., Friedl, M.A., 2020. Continental-scale land surface phenology from harmonized Landsat 8 and Sentinel-2 imagery. Remote Sens. Environ. 240, 111685. https://doi.org/10.1016/j.rse.2020.111685.

Buchner, J., Yin, H., Frantz, D., Kuemmerle, T., Askerov, E., Bakuradze, T., Bleyhl, B., Elizbarashvili, N., Komarova, A., Lewińska, K.E., Rizayeva, A., Sayadyan, H., Tan, B., Tepanosyan, G., Zazanashvili, N., Radeloff, V.C., 2020. Land-cover change in the Caucasus Mountains since 1987 based on the topographic correction of multi-temporal Landsat composites. Remote Sens. Environ. 248, 111967. https://doi.org/10.1016/j.rse.2020.111967.

Bullock, E.L., Woodcock, C.E., Olofsson, P., 2020. Monitoring tropical forest degradation using spectral unmixing and Landsat time series analysis. Remote Sens. Environ. Time Series Analysis with High Spatial Resolution Imagery 238, 110968. https://doi.org/10.1016/j.rse.2018.11.011.

Bundesanstalt für Geowissenschaften und Rohstoffe (BGR), 2018. Bodenübersichtskarte der Bundesrepublik Deutschland 1:200.000 (BÜK200).

Buras, A., Rammig, A., Zang, C.S., 2020. Quantifying impacts of the 2018 drought on European ecosystems in comparison to 2003. Biogeosciences 17, 1655–1672. https://doi.org/10.5194/bg-17-1655-2020.

Buschmann, C., Röder, N., Berglund, K., Berglund, Ö., Lærke, P.E., Maddison, M., Mander, Ü., Myllys, M., Osterburg, B., van den Akker, J.J.H., 2020. Perspectives on agriculturally used drained peat soils: comparison of the socioeconomic and ecological business environments of six European regions. Land Use Policy 90, 104181. https://doi.org/10.1016/j.landusepol.2019.104181.

Buttler, A., Mariotte, P., Meisser, M., Guillaume, T., Signarbieux, C., Vitra, A., Preux, S., Mercier, G., Quezada, J., Bragazza, L., Gavazov, K., 2019. Drought-induced decline of productivity in the dominant grassland species Lolium perenne L. depends on soil type and prevailing climatic conditions. Soil Biol. Biochem. 132, 47–57. https://doi.org/10.1016/j.soilbio.2019.01.026.

Chang, J., Ciais, P., Viovy, N., Soussana, J.-F., Klumpp, K., Sultan, B., 2017. Future productivity and phenology changes in European grasslands for different warming levels: implications for grassland management and carbon balance. Carb. Bal. Manag. 12, 11. https://doi.org/10.1186/s13021-017-0079-8.

Ciais, Ph., Reichstein, M., Viovy, N., Granier, A., Ogée, J., Allard, V., Aubinet, M., Buchmann, N., Bernhofer, Chr, Carrara, A., Chevallier, F., De Noblet, N., Friend, A. D., Friedlingstein, P., Grünwald, T., Heinesch, B., Keronen, P., Knohl, A., Krinner, G., Loustau, D., Manca, G., Matteucci, G., Miglietta, F., Ourcival, J.M., Papale, D., Pilegaard, K., Rambal, S., Seufert, G., Soussana, J.F., Sanz, M.J., Schulze, E.D., Vesala, T., Valentini, R., 2005. Europe-wide reduction in primary productivity caused by the heat and drought in 2003. Nature 437, 529–533. https://doi.org/10.1038/nature03972.

Coates, A.R., Dennison, P.E., Roberts, D.A., Roth, K.L., 2015. Monitoring the impacts of severe drought on Southern California chaparral species using Hyperspectral and thermal infrared imagery. Remote Sens. 7, 14276–14291. https://doi.org/10.3390/rs71114276.

Cooper, S., Okujeni, A., Jänicke, C., Clark, M., van der Linden, S., Hostert, P., 2020. Disentangling fractional vegetation cover: regression-based unmixing of simulated spaceborne imaging spectroscopy data. Remote Sens. Environ. 246, 111856. https://doi.org/10.1016/j.rse.2020.111856.

Corbane, C., Güttler, F., Alleaume, S., Ienco, D., Teisseire, M., 2014. Monitoring the phenology of mediterranean natural habitats with multispectral sensors — an analysis based on multiseasonal field spectra. IEEE Geosci. Remote Sens. Symp. 2014, 3934–3937. https://doi.org/10.1109/IGARSS.2014.6947345.

Cremonese, E., Filippa, G., Galvagno, M., Siniscalco, C., Oddi, L., Morra di Cella, U., Migliavacca, M., 2017. Heat wave hinders green wave: the impact of climate extreme on the phenology of a mountain grassland. Agric. For. Meteorol. 247, 320–330. https://doi.org/10.1016/j.agrformet.2017.08.016.

Daughtry, C.S.T., Hunt, E.R., 2008. Mitigating the effects of soil and residue water contents on remotely sensed estimates of crop residue cover. Remote Sens. Environ. Remote Sensing Data Assimilation Special Issue 112, 1647–1657. https://doi.org/10.1016/j.rse.2007.08.006.

Daughtry, C.S.T., Hunt, E.R., Doraiswamy, P.C., McMurtrey, J.E., 2005. Remote sensing the spatial distribution of crop residues. Agron. J. 97, 864–871. https://doi.org/10.2134/agronj2003.0291.

de Beurs, K.M., Henebry, G.M., Owsley, B.C., Sokolik, I.N., 2018. Large scale climate oscillation impacts on temperature, precipitation and land surface phenology in Central Asia. Environ. Res. Lett. 13, 065018 https://doi.org/10.1088/1748-9326/aac4d0.

De Boeck, H.J., Dreesen, F.E., Janssens, I.A., Nijs, I., 2011. Whole-system responses of experimental plant communities to climate extremes imposed in different seasons. New Phytol. 189, 806–817. https://doi.org/10.1111/j.1469-8137.2010.03515.x.

Delegido, J., Verrelst, J., Rivera, J.P., Ruiz-Verdú, A., Moreno, J., 2015. Brown and green LAI mapping through spectral indices. Int. J. Appl. Earth Obs. Geoinf. 35, 350–358. https://doi.org/10.1016/j.jag.2014.10.001.

Deléglise, C., Meisser, M., Mosimann, E., Spiegelberger, T., Signarbieux, C., Jeangros, B., Buttler, A., 2015. Drought-induced shifts in plants traits, yields and nutritive value under realistic grazing and mowing managements in a mountain grassland. Agric. Ecosyst. Environ. 213, 94–104. https://doi.org/10.1016/j.agee.2015.07.020.

Dennison, P.E., Qi, Y., Meerdink, S.K., Kokaly, R.F., Thompson, D.R., Daughtry, C.S.T., Quemada, M., Roberts, D.A., Gader, P.D., Wetherley, E.B., Numata, I., Roth, K.L., 2019. Comparison of methods for modeling fractional cover using simulated satellite hyperspectral imager spectra. Remote Sens. 11, 2072. https://doi.org/10.3390/rs11182072.

Didan, K., 2015a. MOD13Q1 MODIS/Terra Vegetation Indices 16-Day L3 Global 250m SIN Grid V006. https://doi.org/10.5067/MODIS/MOD13Q1.006.

Didan, K., 2015b. MYD13Q1 MODIS/Aqua Vegetation Indices 16-Day L3 Global 250m SIN Grid V006. https://doi.org/10.5067/MODIS/MYD13Q1.006.

Drouard, M., Kornhuber, K., Woollings, T., 2019. Disentangling dynamic contributions to summer 2018 anomalous weather over Europe. Geophys. Res. Lett. 46, 12537–12546. https://doi.org/10.1029/2019GL084601.

Drusch, M., Del Bello, U., Carlier, S., Colin, O., Fernandez, V., Gascon, F., Hoersch, B., Isola, C., Laberinti, P., Martimort, P., Meygret, A., Spoto, F., Sy, O., Marchese, F., Bargellini, P., 2012. Sentinel-2: ESA's optical high-resolution mission for GMES operational services. Remote Sens. Environ. 120, 25–36. https://doi.org/10.1016/j.rse.2011.11.026.

DWD Climate Data Center (CDC), 2020a. Monthly Grids of the Accumulated Potential Evapotranspiration Over Grass.

DWD Climate Data Center (CDC), 2020b. Grids of Monthly Total Precipitation Over Germany.

Eckelmann, W., Sponagel, H., Grottenthaler, W., Hartmann, K.-J., Hartwich, R., Janetzko, P., Joisten, H., Kühn, D., Sabel, K.-J., Traidl, R., 2005. Bodenkundliche Kartieranleitung. Bundesanstalt für Geowissenschaften und Rohstoffe in Zusammenarbeit mit den Staatlichen Geologischen Diensten. Hannover, Germany.

Elmore, A.J., Mustard, J.F., Manning, S.J., Lobell, D.B., 2000. Quantifying vegetation change in semiarid environments: precision and accuracy of spectral mixture analysis and the normalized difference vegetation index. Remote Sens. Environ. 73, 87–102. https://doi.org/10.1016/S0034-4257(00)00100-0.

Enke, W., Deutschländer, T., Schneider, F., Küchler, W., 2005. Results of five regional climate studies applying a weather pattern based downscaling method to ECHAM4 climate simulation. Metz 14, 247–257. https://doi.org/10.1127/0941-2948/2005/0028.

Estel, S., Mader, S., Levers, C., Verburg, P.H., Baumann, M., Kuemmerle, T., 2018. Combining satellite data and agricultural statistics to map grassland management intensity in Europe. Environ. Res. Lett. 13 https://doi.org/10.1088/1748-9326/aacc7a.

European Space Agency (ESA), 2020. S2 MPC L1C Data Quality Report (No. Issue 55 Ref. S2-PDGS-MPC-DQR).

Frantz, D., 2019. FORCE—Landsat + Sentinel-2 analysis ready data and beyond. Remote Sens. 11, 1124. https://doi.org/10.3390/rs11091124.

Frantz, D., Röder, A., Stellmes, M., Hill, J., 2016a. An operational radiometric Landsat preprocessing framework for large-area time series applications. IEEE Trans. Geosci. Remote Sens. 54, 3928–3943. https://doi.org/10.1109/TGRS.2016.2530856.

Frantz, D., Stellmes, M., Roder, A., Udelhoven, T., Mader, S., Hill, J., 2016b. Improving the spatial resolution of land surface phenology by fusing medium- and coarse-resolution inputs. IEEE Trans. Geosci. Remote Sens. 54, 4153–4164. https://doi.org/10.1109/TGRS.2016.2537929.

Frantz, D., Haß, E., Uhl, A., Stoffels, J., Hill, J., 2018. Improvement of the Fmask algorithm for Sentinel-2 images: separating clouds from bright surfaces based on parallax effects. Remote Sens. Environ. 215, 471–481. https://doi.org/10.1016/j.rse.2018.04.046.

Gao, X., Huete, A.R., Ni, W., Miura, T., 2000. Optical–biophysical relationships of vegetation spectra without background contamination. Remote Sens. Environ. 74, 609–620. https://doi.org/10.1016/S0034-4257(00)00150-4.

Gastal, F., Lemaire, G., 2015. Defoliation, shoot plasticity, sward structure and herbage utilization in pasture: review of the underlying ecophysiological processes. Agriculture 5, 1146–1171. https://doi.org/10.3390/agriculture5041146.

Ge, J., Meng, B., Liang, T., Feng, Q., Gao, J., Yang, S., Huang, X., Xie, H., 2018. Modeling alpine grassland cover based on MODIS data and support vector machine regression in the headwater region of the Huanghe River, China. Remote Sens. Environ. 218, 162–173. https://doi.org/10.1016/j.rse.2018.09.019.

German Weather Service, 2020. Time Series and Trends [WWW Document]. www.dwd.de/EN/ourservices/zeitreihen/zeitreihen.html.

Gessner, U., Machwitz, M., Conrad, C., Dech, S., 2013. Estimating the fractional cover of growth forms and bare surface in savannas. A multi-resolution approach based on regression tree ensembles. Remote Sens. Environ. 129, 90–102. https://doi.org/10.1016/j.rse.2012.10.026.

Gitelson, A.A., Kaufman, Y.J., Stark, R., Rundquist, D., 2002. Novel algorithms for remote estimation of vegetation fraction. Remote Sens. Environ. 80, 76–87. https://doi.org/10.1016/S0034-4257(01)00289-9.

Grant, K., Kreyling, J., Heilmeier, H., Beierkuhnlein, C., Jentsch, A., 2014. Extreme weather events and plant–plant interactions: shifts between competition and facilitation among grassland species in the face of drought and heavy rainfall. Ecol. Res. 29, 991–1001. https://doi.org/10.1007/s11284-014-1187-5.

Green, R.O., 2018. Global VSWIR imaging spectroscopy and the 2017 decadal survey. In: IGARSS 2018–2018 IEEE International Geoscience and Remote Sensing Symposium. Presented at the IGARSS 2018–2018 IEEE International Geoscience and Remote Sensing Symposium, pp. 183–185. https://doi.org/10.1109/IGARSS.2018.8518744.

Griffiths, P., Nendel, C., Pickert, J., Hostert, P., 2020. Towards national-scale characterization of grassland use intensity from integrated Sentinel-2 and Landsat time series. Remote Sens. Environ. 1–12. https://doi.org/10.1016/j.rse.2019.03.017.

Grünewald, U., 2001. Water resources management in river catchments influenced by lignite mining. Ecol. Eng. 17, 143–152. https://doi.org/10.1016/S0925-8574(00)00154-3.

Guerschman, J.P., Hill, M.J., Renzullo, L.J., Barrett, D.J., Marks, A.S., Botha, E.J., 2009. Estimating fractional cover of photosynthetic vegetation, non-photosynthetic vegetation and bare soil in the Australian tropical savanna region upscaling the EO-1 Hyperion and MODIS sensors. Remote Sens. Environ. 113, 928–945. https://doi.org/10.1016/j.rse.2009.01.006.

Guerschman, J.P., Scarth, P.F., McVicar, T.R., Renzullo, L.J., Malthus, T.J., Stewart, J.B., Rickards, J.E., Trevithick, R., 2015. Assessing the effects of site heterogeneity and soil properties when unmixing photosynthetic vegetation, non-photosynthetic vegetation and bare soil fractions from Landsat and MODIS data. Remote Sens. Environ. 161, 12–26. https://doi.org/10.1016/j.rse.2015.01.021.

Guerschman, J.P., Hill, M.J., Leys, J., Heidenreich, S., 2020. Vegetation cover dependence on accumulated antecedent precipitation in Australia: relationships with photosynthetic and non-photosynthetic vegetation fractions. Remote Sens. Environ. 240, 111670. https://doi.org/10.1016/j.rse.2020.111670.

Hari, V., Rakovec, O., Markonis, Y., Hanel, M., Kumar, R., 2020. Increased future occurrences of the exceptional 2018–2019 Central European drought under global warming. Sci. Rep. 10, 12207. https://doi.org/10.1038/s41598-020-68872-9.

He, Y., Yang, J., Guo, X., 2020. Green vegetation cover dynamics in a heterogeneous grassland: spectral unmixing of Landsat time series from 1999 to 2014. Remote Sens. 12, 3826. https://doi.org/10.3390/rs12223826.
Hejcman, M., Hejcmanová, P., Pavlů, V., Beneš, J., 2013. Origin and history of grasslands in central europe - a review. Grass Forage Sci. 68, 345–363. https://doi.org/10.1111/gfs.12066.
Hellwig, J., de Graaf, I.E.M., Weiler, M., Stahl, K., 2020. Large-scale assessment of delayed groundwater responses to drought. Water Resour. Res. 56 https://doi.org/10.1029/2019WR025441 e2019WR025441.
Henebry, G.M., 2019. Methodology II: Remote sensing of change in grasslands. In: Gibson, D.J., Newman, J.A. (Eds.), Grasslands and Climate Change. Ecological Reviews. Cambridge University Press, Cambridge, pp. 40–64. https://doi.org/10.1017/9781108163941.005.
Hill, M.J., Zhou, Q., Sun, Q., Schaaf, C.B., Southworth, J., Mishra, N.B., Gibbes, C., Bunting, E., Christiansen, T.B., Crews, K.A., 2016. Dynamics of the relationship between NDVI and SWIR32 vegetation indices in southern Africa: implications for retrieval of fractional cover from MODIS data. Int. J. Remote Sens. 37, 1476–1503. https://doi.org/10.1080/01431161.2016.1154225.
Hill, M.J., Zhou, Q., Sun, Q., Schaaf, C.B., Palace, M., 2017. Relationships between vegetation indices, fractional cover retrievals and the structure and composition of Brazilian Cerrado natural vegetation. Int. J. Remote Sens. 38, 874–905. https://doi.org/10.1080/01431161.2016.1271959.
Hofer, D., Suter, M., Haughey, E., Finn, J.A., Hoekstra, N.J., Buchmann, N., Lüscher, A., 2016. Yield of temperate forage grassland species is either largely resistant or resilient to experimental summer drought. J. Appl. Ecol. 53, 1023–1034. https://doi.org/10.1111/1365-2664.12694.
Horton, D.E., Johnson, N.C., Singh, D., Swain, D.L., Rajaratnam, B., Diffenbaugh, N.S., 2015. Contribution of changes in atmospheric circulation patterns to extreme temperature trends. Nature 522, 465–469. https://doi.org/10.1038/nature14550.
Huber, S., Huber, B., Stahl, S., Schmid, C., Reisch, C., 2017. Species diversity of remnant calcareous grasslands in south eastern Germany depends on litter cover and landscape structure. Acta Oecol. 83, 48–55. https://doi.org/10.1016/j.actao.2017.06.011.
Huete, A.R., Jackson, R.D., Post, D.F., 1985. Spectral response of a plant canopy with different soil backgrounds. Remote Sens. Environ. 17, 37–53. https://doi.org/10.1016/0034-4257(85)90111-7.
Ingrisch, J., Karlowsky, S., Anadon-Rosell, A., Hasibeder, R., König, A., Augusti, A., Gleixner, G., Bahn, M., 2018. Land use alters the drought responses of productivity and CO2 fluxes in mountain grassland. Ecosystems 21, 689–703. https://doi.org/10.1007/s10021-017-0178-0.
Ji, L., Peters, A.J., 2003. Assessing vegetation response to drought in the northern Great Plains using vegetation and drought indices. Remote Sens. Environ. 87, 85–98. https://doi.org/10.1016/S0034-4257(03)00174-3.
Ji, C., Li, X., Wei, H., Li, S., 2020. Comparison of different multispectral sensors for photosynthetic and non-photosynthetic vegetation-fraction retrieval. Remote Sens. 12, 115. https://doi.org/10.3390/rs12010115.
Jin, H., Jönsson, A.M., Olsson, C., Lindström, J., Jönsson, P., Eklundh, L., 2019. New satellite-based estimates show significant trends in spring phenology and complex sensitivities to temperature and precipitation at northern European latitudes. Int. J. Biometeorol. 63, 763–775. https://doi.org/10.1007/s00484-019-01690-5.
Kaiser, T., Leipnitz, W., Käding, H., Haberstock, W., Glemnitz, M., 2001. Die räumliche herleitung der Grünland vegetation eines Niedermoorgebietes anhand von Standort- und Nutzungskarten. Arch. Agron. Soil Sci. 46, 91–101. https://doi.org/10.1080/03650340109366162.
Klaus, V.H., Friedritz, L., Hamer, U., Kleinebecker, T., 2020. Drought boosts risk of nitrate leaching from grassland fertilisation. Sci. Total Environ. 726, 137877. https://doi.org/10.1016/j.scitotenv.2020.137877.
Kogan, F.N., 1995. Droughts of the late 1980s in the United States as derived from NOAA polar-orbiting satellite data. Bull. Am. Meteorol. Soc. 76, 655–668. https://doi.org/10.1175/1520-0477(1995)076<0655:DOTLIT>2.0.CO;2.
Kolecka, N., Ginzler, C., Pazur, R., Price, B., Verburg, P.H., 2018. Regional scale mapping of grassland mowing frequency with Sentinel-2 time series. Remote Sens. 10 https://doi.org/10.3390/rs10081221.
Kowalski, K., Senf, C., Hostert, P., Pflugmacher, D., 2020. Characterizing spring phenology of temperate broadleaf forests using Landsat and Sentinel-2 time series. Int. J. Appl. Earth Obs. Geoinf. 92, 102172. https://doi.org/10.1016/j.jag.2020.102172.
Kuemmerle, T., Levers, C., Erb, K., Estel, S., Jepsen, M.R., Müller, D., Plutzar, C., Stürck, J., Verkerk, P.J., Verburg, P.H., Reenberg, A., 2016. Hotspots of land use change in Europe. Environ. Res. Lett. 11, 064020 https://doi.org/10.1088/1748-9326/11/6/064020.
Landesamt für Ländliche Entwicklung, Landwirtschaft und Flurneuordnung (LELF), 2014. Nutzung und Schutz grundwasserbeeinflusster Böden Brandenburgs.
Landesumweltamt Brandenburg (LUA), 2004. Leitfaden zur Renaturierung von Feuchtgebieten in Brandenburg (No. 50), Studien und Tagungsberichte des Landesumweltamtes.
Lehnert, L.W., Meyer, H., Wang, Y., Miehe, G., Thies, B., Reudenbach, C., Bendix, J., 2015. Retrieval of grassland plant coverage on the Tibetan Plateau based on a multi-scale, multi-sensor and multi-method approach. Remote Sens. Environ. 164, 197–207. https://doi.org/10.1016/j.rse.2015.04.020.
Lewińska, K.E., Hostert, P., Buchner, J., Bleyhl, B., Radeloff, V.C., 2020. Short-term vegetation loss versus decadal degradation of grasslands in the caucasus based on cumulative endmember fractions. Remote Sens. Environ. 248, 111969. https://doi.org/10.1016/j.rse.2020.111969.
Li, F., Chen, J.Q., Zeng, Y., Wu, B.F., Zhang, X.Q., 2018. Renewed estimates of grassland aboveground biomass showing drought impacts. J. Geophys. Res. Biogeosci. 123, 138–148. https://doi.org/10.1002/2017JG004255.
Lippitt, C.L., Stow, D.A., Roberts, D.A., Coulter, L.L., 2018. Multidate MESMA for monitoring vegetation growth forms in southern California shrublands. Int. J. Remote Sens. 39, 655–683. https://doi.org/10.1080/01431161.2017.1388936.
Liu, J., Pattey, E., Jégo, G., 2012. Assessment of vegetation indices for regional crop green LAI estimation from Landsat images over multiple growing seasons. Remote Sens. Environ. 123, 347–358. https://doi.org/10.1016/j.rse.2012.04.002.
Lopatin, J., Fassnacht, F.E., Kattenborn, T., Schmidtlein, S., 2017. Mapping plant species in mixed grassland communities using close range imaging spectroscopy. Remote Sens. Environ. 201, 12–23. https://doi.org/10.1016/j.rse.2017.08.031.
López-Moreno, J.I., Vicente-Serrano, S.M., 2008. Positive and negative phases of the wintertime North Atlantic oscillation and drought occurrence over Europe: a multitemporal-scale approach. J. Clim. 21, 1220–1243. https://doi.org/10.1175/2007JCLI1739.1.
Ma, X., Huete, A., Yu, Q., Coupe, N.R., Davies, K., Broich, M., Ratana, P., Beringer, J., Hutley, L.B., Cleverly, J., Boulain, N., Eamus, D., 2013. Spatial patterns and temporal dynamics in savanna vegetation phenology across the north Australian tropical transect. Remote Sens. Environ. 139, 97–115. https://doi.org/10.1016/j.rse.2013.07.030.
Mariano, D.A., dos Santos, C.A.C., Wardlow, B.D., Anderson, M.C., Schiltmeyer, A.V., Tadesse, T., Svoboda, M.D., 2018. Use of remote sensing indicators to assess effects of drought and human-induced land degradation on ecosystem health in Northeastern Brazil. Remote Sens. Environ. 213, 129–143. https://doi.org/10.1016/j.rse.2018.04.048.
Mariotte, P., Vandenberghe, C., Kardol, P., Hagedorn, F., Buttler, A., 2013. Subordinate plant species enhance community resistance against drought in semi-natural grasslands. J. Ecol. 101, 763–773. https://doi.org/10.1111/1365-2745.12064.
McKee, T.B., Doesken, N.J., Kleist, J., 1993. The relationship of drought frequency and duration to time scales. Proceedings of the eighth conference on applied climatology, American Meteorological Society 179–184.
Melaas, E.K., Friedl, M.A., Zhu, Z., 2013. Detecting interannual variation in deciduous broadleaf forest phenology using Landsat TM/ETM+ data. Remote Sens. Environ. 132, 176–185. https://doi.org/10.1016/j.rse.2013.01.011.
Meyer, T., Okin, G.S., 2015. Evaluation of spectral unmixing techniques using MODIS in a structurally complex savanna environment for retrieval of green vegetation, nonphotosynthetic vegetation, and soil fractional cover. Remote Sens. Environ. 161, 122–130. https://doi.org/10.1016/j.rse.2015.02.013.
Montorio, R., Pérez-Cabello, F., Borini Alves, D., García-Martín, A., 2020. Unitemporal approach to fire severity mapping using multispectral synthetic databases and random forests. Remote Sens. Environ. 249, 112025. https://doi.org/10.1016/j.rse.2020.112025.
Nagler, P.L., Daughtry, C.S.T., Goward, S.N., 2000. Plant litter and soil reflectance. Remote Sens. Environ. 71, 207–215. https://doi.org/10.1016/S0034-4257(99)00082-6.
Nieke, J., Rast, M., 2018. Towards the copernicus hyperspectral imaging mission for the environment (CHIME). In: IGARSS 2018–2018 IEEE International Geoscience and Remote Sensing Symposium. Presented at the IGARSS 2018–2018 IEEE International Geoscience and Remote Sensing Symposium. IEEE, Valencia, pp. 157–159. https://doi.org/10.1109/IGARSS.2018.8518384.
Numata, I., Roberts, D.A., Chadwick, O.A., Schimel, J., Sampaio, F.R., Leonidas, F.C., Soares, J.V., 2007. Characterization of pasture biophysical properties and the impact of grazing intensity using remotely sensed data. Remote Sens. Environ. 109, 314–327. https://doi.org/10.1016/j.rse.2007.01.013.
Okujeni, A., van der Linden, S., Tits, L., Somers, B., Hostert, P., 2013. Support vector regression and synthetically mixed training data for quantifying urban land cover. Remote Sens. Environ. 137, 184–197. https://doi.org/10.1016/j.rse.2013.06.007.
Okujeni, A., van der Linden, S., Suess, S., Hostert, P., 2017. Ensemble learning from synthetically mixed training data for quantifying urban land cover with support vector regression. IEEE J. Sel. Top. Appl. Earth Observ. Remote Sens. 10, 1640–1650. https://doi.org/10.1109/JSTARS.2016.2634859.
Okujeni, A., Canters, F., Cooper, S.D., Degerickx, J., Heiden, U., Hostert, P., Priem, F., Roberts, D.A., Somers, B., van der Linden, S., 2018. Generalizing machine learning regression models using multi-site spectral libraries for mapping vegetation-impervious-soil fractions across multiple cities. Remote Sens. Environ. 216, 482–496. https://doi.org/10.1016/j.rse.2018.07.011.
Okujeni, A., Jänicke, C., Cooper, S., Frantz, D., Hostert, P., Clark, M., Segl, K., van der Linden, S., 2021. Multi-season unmixing of vegetation class fractions across diverse Californian ecoregions using simulated spaceborne imaging spectroscopy data. Remote Sens. Environ. 112558 https://doi.org/10.1016/j.rse.2021.112558.
Punalekar, S.M., Verhoef, A., Quaife, T.L., Humphries, D., Bermingham, L., Reynolds, C. K., 2018. Application of Sentinel-2A data for pasture biomass monitoring using a physically based radiative transfer model. Remote Sens. Environ. 218, 207–220. https://doi.org/10.1016/j.rse.2018.09.028.
Reinermann, S., Gessner, U., Asam, S., Kuenzer, C., Dech, S., 2019. The effect of droughts on vegetation condition in Germany: an analysis based on two decades of satellite earth observation time series and crop yield statistics. Remote Sens. 11, 1783. https://doi.org/10.3390/rs11151783.
Reinermann, S., Asam, S., Kuenzer, C., 2020. Remote sensing of grassland production and management—a review. Remote Sens. 12, 1949. https://doi.org/10.3390/rs12121949.
Roberts, D.A., Gardner, M., Church, R., Ustin, S., Scheer, G., Green, R.O., 1998. Mapping chaparral in the Santa Monica Mountains using multiple endmember spectral mixture models. Remote Sens. Environ. 65, 267–279. https://doi.org/10.1016/S0034-4257(98)00037-6.

Roberts, D.A., Quattrochi, D.A., Hulley, G.C., Hook, S.J., Green, R.O., 2012. Synergies between VSWIR and TIR data for the urban environment: an evaluation of the potential for the Hyperspectral Infrared Imager (HyspIRI) decadal survey mission. Remote Sens. Environ. 117, 83–101. https://doi.org/10.1016/j.rse.2011.07.021.

Röder, A., Udelhoven, Th., Hill, J., del Barrio, G., Tsiourlis, G., 2008. Trend analysis of Landsat-TM and -ETM+ imagery to monitor grazing impact in a rangeland ecosystem in Northern Greece. Remote Sens. Environ. 112, 2863–2875. https://doi.org/10.1016/j.rse.2008.01.018.

Rufin, P., Frantz, D., Yan, L., Hostert, P., 2020. Operational coregistration of the sentinel-2A/B image archive using multitemporal Landsat spectral averages. IEEE Geosci. Remote Sensing Lett. 1–5. https://doi.org/10.1109/LGRS.2020.2982245.

Samaniego, L., Kumar, R., Attinger, S., 2010. Multiscale parameter regionalization of a grid-based hydrologic model at the mesoscale. Water Resour. Res. 46 https://doi.org/10.1029/2008WR007327.

Samaniego, L., Thober, S., Kumar, R., Wanders, N., Rakovec, O., Pan, M., Zink, M., Sheffield, J., Wood, E.F., Marx, A., 2018. Anthropogenic warming exacerbates European soil moisture droughts. Nat. Clim. Chang. 8, 421–426. https://doi.org/10.1038/s41558-018-0138-5.

Sanaullah, M., Chabbi, A., Lemaire, G., Charrier, X., Rumpel, C., 2010. How does plant leaf senescence of grassland species influence decomposition kinetics and litter compounds dynamics? Nutr. Cycl. Agroecosyst. 88, 159–171. https://doi.org/10.1007/s10705-009-9323-2.

Schug, F., Frantz, D., Okujeni, A., van der Linden, S., Hostert, P., 2020. Mapping urban-rural gradients of settlements and vegetation at national scale using Sentinel-2 spectral-temporal metrics and regression-based unmixing with synthetic training data. Remote Sens. Environ. 246, 111810. https://doi.org/10.1016/j.rse.2020.111810.

Schuldt, B., Buras, A., Arend, M., Vitasse, Y., Beierkuhnlein, C., Damm, A., Gharun, M., Grams, T.E.E., Hauck, M., Hajek, P., Hartmann, H., Hiltbrunner, E., Hoch, G., Holloway-Phillips, M., Körner, C., Larysch, E., Lübbe, T., Nelson, D.B., Rammig, A., Rigling, A., Rose, L., Ruehr, N.K., Schumann, K., Weiser, F., Werner, C., Wohlgemuth, T., Zang, C.S., Kahmen, A., 2020. A first assessment of the impact of the extreme 2018 summer drought on Central European forests. Basic Appl. Ecol. 45, 86–103. https://doi.org/10.1016/j.baae.2020.04.003.

Schwieder, M., Leitão, P.J., da Cunha Bustamante, M.M., Ferreira, L.G., Rabe, A., Hostert, P., 2016. Mapping Brazilian savanna vegetation gradients with Landsat time series. Int. J. Appl. Earth Obs. Geoinf. 52, 361–370. https://doi.org/10.1016/j.jag.2016.06.019.

Schwieder, M., Buddeberg, M., Kowalski, K., Pfoch, K., Bartsch, J., Bach, H., Pickert, J., Hostert, P., 2020. Estimating grassland parameters from Sentinel-2: a model comparison study. PFG. https://doi.org/10.1007/s41064-020-00120-1.

Seneviratne, S.I., Nicholls, N., Easterling, D., Goodess, C.M., Kanae, S., Kossin, J., Luo, Y., Marengo, J., McInnes, K., Rahimi, M., Reichstein, M., Sorteberg, A., Vera, C., Zhang, X., Rusticucci, M., Semenov, V., Alexander, L.V., Allen, S., Benito, G., Cavazos, T., Clague, J., Conway, D., Della-Marta, P.M., Gerber, M., Gong, S., Goswami, B.N., Hemer, M., Huggel, C., van den Hurk, B., Kharin, V.V., Kitoh, A., Tank, A.M.G.K., Li, G., Mason, S., McGuire, W., van Oldenborgh, G.J., Orlowsky, B., Smith, S., Thiaw, W., Velegrakis, A., Yiou, P., Zhang, T., Zhou, T., Zwiers, F.W., 2012. Changes in climate extremes and their impacts on the natural physical environment. In: Field, C.B., Barros, V., Stocker, T.F., Dahe, Q. (Eds.), Managing the Risks of Extreme Events and Disasters to Advance Climate Change Adaptation. Cambridge University Press, Cambridge, pp. 109–230. https://doi.org/10.1017/CBO9781139177245.006.

Senf, C., Pflugmacher, D., Heurich, M., Krueger, T., 2017. A Bayesian hierarchical model for estimating spatial and temporal variation in vegetation phenology from Landsat time series. Remote Sens. Environ. 194, 155–160. https://doi.org/10.1016/j.rse.2017.03.020.

Senf, C., Laštovička, J., Okujeni, A., Heurich, M., van der Linden, S., 2020. A generalized regression-based unmixing model for mapping forest cover fractions throughout three decades of Landsat data. Remote Sens. Environ. 240, 111691. https://doi.org/10.1016/j.rse.2020.111691.

Smit, H.J., Metzger, M.J., Ewert, F., 2008. Spatial distribution of grassland productivity and land use in Europe. Agric. Syst. 98, 208–219. https://doi.org/10.1016/j.agsy.2008.07.004.

Smola, A.J., Schölkopf, B., 2004. A tutorial on support vector regression. Stat. Comput. 14, 199–222. https://doi.org/10.1023/B:STCO.0000035301.49549.88.

Soussana, J.-F., Lüscher, A., 2007. Temperate grasslands and global atmospheric change: a review. Grass Forage Sci. 62, 127–134. https://doi.org/10.1111/j.1365-2494.2007.00577.x.

Souza, C.M., Roberts, D.A., Cochrane, M.A., 2005. Combining spectral and spatial information to map canopy damage from selective logging and forest fires. Remote Sens. Environ. 98, 329–343. https://doi.org/10.1016/j.rse.2005.07.013.

Statistisches Amt Mecklenburg-Vorpommern, 2018. Ernteberichterstattung über Feldfrüchte und Grünland in Mecklenburg-Vorpommern.

Statistisches Bundesamt, 2019. Statistisches Jahrbuch Deutschland und Internationales.

Stumpf, F., Schneider, M.K., Keller, A., Mayr, A., Rentschler, T., Meuli, R.G., Schaepman, M., Liebisch, F., 2020. Spatial monitoring of grassland management using multi-temporal satellite imagery. Ecol. Indic. 113, 106201. https://doi.org/10.1016/j.ecolind.2020.106201.

Suess, S., van der Linden, S., Okujeni, A., Griffiths, P., Leitão, P.J., Schwieder, M., Hostert, P., 2018. Characterizing 32 years of shrub cover dynamics in southern Portugal using annual Landsat composites and machine learning regression modeling. Remote Sens. Environ. 219, 353–364. https://doi.org/10.1016/j.rse.2018.10.004.

Tanneberger, F., Schröder, C., Hohlbein, M., Lenschow, Uwe, Permien, T., Wichmann, S., Wichtmann, W., 2020. Climate change mitigation through land use on rewetted peatlands – cross-sectoral spatial planning for paludiculture in Northeast Germany. Wetlands 40, 2309–2320. https://doi.org/10.1007/s13157-020-01310-8.

Team, AppEEARS, 2021. Application for Extracting and Exploring Analysis Ready Samples (AppEEARS). NASA EOSDIS Land Processes Distributed Active Archive Center (LP DAAC), USGS/Earth Resources Observation and Science (EROS) Center, Sioux Falls, South Dakota, USA.

Tian, J., Su, S., Tian, Q., Zhan, W., Xi, Y., Wang, N., 2021. A novel spectral index for estimating fractional cover of non-photosynthetic vegetation using near-infrared bands of sentinel satellite. Int. J. Appl. Earth Obs. Geoinf. 101, 102361. https://doi.org/10.1016/j.jag.2021.102361.

Török, P., Kapocsi, I., Deák, B., 2012. Conservation and management of alkali grassland biodiversity in Central-Europe. In: Grasslands: Types, Biodiversity and Impacts, Environmental Health : Physical, Chemical and Biological Factors. Nova Science Publishers, Hauppauge, N.Y.

Tucker, C.T., 1979. Red and photographic infrared linear combinations for monitoring vegetation. Remote Sens. Environ. 8, 127–150.

van der Linden, S., Rabe, A., Held, M., Jakimow, B., Leitão, P., Okujeni, A., Schwieder, M., Suess, S., Hostert, P., 2015. The EnMAP-box—A toolbox and application programming interface for EnMAP data processing. Remote Sens. 7, 11249–11266. https://doi.org/10.3390/rs70911249.

Vicente-Serrano, S.M., Beguería, S., López-Moreno, J.I., 2010. A multiscalar drought index sensitive to global warming: the standardized precipitation evapotranspiration index. J. Clim. 23, 1696–1718. https://doi.org/10.1175/2009JCLI2909.1.

Vogel, A., Scherer-Lorenzen, M., Weigelt, A., 2012. Grassland resistance and resilience after drought depends on management intensity and species richness. PLoS One 7, e36992. https://doi.org/10.1371/journal.pone.0036992.

Walter, J., Hein, R., Beierkuhnlein, C., Hammerl, V., Jentsch, A., Schädler, M., Schuerings, J., Kreyling, J., 2013. Combined effects of multifactor climate change and land-use on decomposition in temperate grassland. Soil Biol. Biochem. 60, 10–18. https://doi.org/10.1016/j.soilbio.2013.01.018.

Wang, G., Wang, J., Zou, X., Chai, G., Wu, M., Wang, Z., 2019a. Estimating the fractional cover of photosynthetic vegetation, non-photosynthetic vegetation and bare soil from MODIS data: assessing the applicability of the NDVI-DFI model in the typical Xilingol grasslands. Int. J. Appl. Earth Obs. Geoinf. 76, 154–166. https://doi.org/10.1016/j.jag.2018.11.006.

Wang, J., Xiao, X., Bajgain, R., Starks, P., Steiner, J., Doughty, R.B., Chang, Q., 2019b. Estimating leaf area index and aboveground biomass of grazing pastures using Sentinel-1, Sentinel-2 and Landsat images. ISPRS J. Photogramm. Remote Sens. 154, 189–201. https://doi.org/10.1016/j.isprsjprs.2019.06.007.

Wellstein, C., Poschlod, P., Gohlke, A., Chelli, S., Campetella, G., Rosbakh, S., Canullo, R., Kreyling, J., Jentsch, A., Beierkuhnlein, C., 2017. Effects of extreme drought on specific leaf area of grassland species: a meta-analysis of experimental studies in temperate and sub-Mediterranean systems. Glob. Chang. Biol. 23, 2473–2481. https://doi.org/10.1111/gcb.13662.

West, H., Quinn, N., Horswell, M., 2019. Remote sensing for drought monitoring & impact assessment: Progress, past challenges and future opportunities. Remote Sens. Environ. 232, 111291. https://doi.org/10.1016/j.rse.2019.111291.

Wingate, L., Ogée, J., Cremonese, E., Filippa, G., Mizunuma, T., Migliavacca, M., Moisy, C., Wilkinson, M., Moureaux, C., Wohlfahrt, G., Hammerle, A., Hörtnagl, L., Gimeno, C., Porcar-Castell, A., Galvagno, M., Nakaji, T., Morison, J., Kolle, O., Knohl, A., Kutsch, W., Kolari, P., Nikinmaa, E., Ibrom, A., Gielen, B., Eugster, W., Balzarolo, M., Papale, D., Klumpp, K., Köstner, B., Grünwald, T., Joffre, R., Ourcival, J.-M., Hellstrom, M., Lindroth, A., George, C., Longdoz, B., Genty, B., Levula, J., Heinesch, B., Sprintsin, M., Yakir, D., Manise, T., Guyon, D., Ahrends, H., Plaza-Aguilar, A., Guan, J.H., Grace, J., 2015. Interpreting canopy development and physiology using a European phenology camera network at flux sites. Biogeosciences 12, 5995–6015. https://doi.org/10.5194/bg-12-5995-2015.

Wingler, A., Hennessy, D., 2016. Limitation of grassland productivity by low temperature and seasonality of growth. Front. Plant Sci. 7, 1130. https://doi.org/10.3389/fpls.2016.01130.

Wulder, M.A., White, J.C., Loveland, T.R., Woodcock, C.E., Belward, A.S., Cohen, W.B., Fosnight, E.A., Shaw, J., Masek, J.G., Roy, D.P., 2016. The global Landsat archive: status, consolidation, and direction. Remote Sens. Environ. Landsat 8 Science Results 185, 271–283. https://doi.org/10.1016/j.rse.2015.11.032.

Xu, D., Guo, X., Li, Z., Yang, X., Yin, H., 2014. Measuring the dead component of mixed grassland with Landsat imagery. Remote Sens. Environ. 142, 33–43. https://doi.org/10.1016/j.rse.2013.11.017.

Yan, L., Roy, D.P., Zhang, H., Li, J., Huang, H., 2016. An automated approach for sub-pixel registration of Landsat-8 operational land imager (OLI) and Sentinel-2 multi spectral instrument (MSI) imagery. Remote Sens. 8, 520. https://doi.org/10.3390/rs8060520.

Yu, X., Guo, Q., Chen, Q., Guo, X., 2019. Discrimination of senescent vegetation cover from Landsat-8 OLI imagery by spectral unmixing in the northern mixed grasslands. Can. J. Remote. Sens. 45, 192–208. https://doi.org/10.1080/07038992.2019.1605586.

Zhu, Z., Woodcock, C.E., 2012. Object-based cloud and cloud shadow detection in Landsat imagery. Remote Sens. Environ. 118, 83–94. https://doi.org/10.1016/j.rse.2011.10.028.

Zhu, Z., Woodcock, C.E., 2014. Automated cloud, cloud shadow, and snow detection in multitemporal Landsat data: an algorithm designed specifically for monitoring land cover change. Remote Sens. Environ. 152, 217–234. https://doi.org/10.1016/j.rse.2014.06.012.

Zink, M., Samaniego, L., Kumar, R., Thober, S., Mai, J., Schäfer, D., Marx, A., 2016. The German drought monitor. Environ. Res. Lett. 11, 074002 https://doi.org/10.1088/1748-9326/11/7/074002.

Zscheischler, J., Fischer, E.M., 2020. The record-breaking compound hot and dry 2018 growing season in Germany. Weather Climate Extremes 100270. https://doi.org/10.1016/j.wace.2020.100270.

Zwicke, M., Alessio, G.A., Thiery, L., Falcimagne, R., Baumont, R., Rossignol, N., Soussana, J.-F., Picon-Cochard, C., 2013. Lasting effects of climate disturbance on perennial grassland above-ground biomass production under two cutting frequencies. Glob. Chang. Biol. 19, 3435–3448. https://doi.org/10.1111/gcb.12317.